Shallow subsurface deformation along the Pen Branch Fault

in South Carolina: Interpretation from seismic refraction stack sections

by

Leslie Diane Moore

Thesis submitted to the Faculty of the

Virginia Polytechnic Institute and State University

in partial fulfillment of the requirements for the degree of

Master of Science

in

Geophysics

APPROVED:

Cahit Çoruh, Chairman

John K. Costain

Edwin S. Robinson

January, 1997
Blacksburg, Virginia

Keywords: Shallow Refraction, Savannah River Site, Geophysics

Shallow subsurface deformation along the Pen Branch Fault in South Carolina: Interpretation from seismic refraction stack sections

by

Leslie Diane Moore

Cahit Çoruh, Chairman

Geophysics

(ABSTRACT)

The Pen Branch Fault is a reactivated, high angle, reverse basin border fault that dips to southeast from the basement (Triassic-Paleozoic-Precambrian in age) to near vertical through the Atlantic Coastal Plain sediments (Late Cretaceous to Recent in age) of the Savannah River site in South Carolina. The fault movement has occurred through Late Cretaceous to Tertiary. Faulting might penetrate as shallow as the Dry Branch and the Tobacco Road Sand Formations (Late Eocene).

An investigation with high resolution reflection seismic data is undertaken along the Pen Branch Fault. Five of the seismic lines are reprocessed to help in determining the upward depth of penetration of this fault. This is done by utilizing refracted arrivals from the multifold reflection data.

The shallowest refractors (4 - 18 m) imaged have an average velocity of 1700 m/s . All of the lines exhibit events that are not flat lying across the data where the fault is believed to be. The lines possess deformation such as offsets, upwarping and channels. Deformation can be related to the Pen Branch Fault as shallow as 4 m from the surface. Displacements along the lines vary from 1 m up to 5 m. Reverse sense of motion is mainly exhibited along the fault zone that is covered by this study. The events resolved portray the Pen Branch Fault in a fault zone of subparallel faults and splays.

Acknowledgments

I would like to thank Dr. Cahit Çoruh for serving as my advisor and Dr. John K. Costain and Dr. Edwin S. Robinson for serving as my committee members. Special thanks to Mildred Memitt for her help with my project and Bob Montgomery and John Wonderley for keeping the computer systems from being totally useless and Randy Link for getting the plotters rolling again.

I extend my appreciation to my family and to Rod, Wendi, Jeff, Sara, Jennifer, Ginger and all the rest for all they have done and for keeping me going and not letting me give up. I dedicate this work to my parents for their encouragement and support during all my educational endeavors.

Financial support was received from the Department of Geological Sciences, Texaco and Chevron in the form of assistantships and fellowships.

Table Of Contents

List of Figures

List of Tables

Introduction

The purpose of the study is to test the use of refraction stack sections derived from seismic reflection data recorded with an off-end spread to determine shallow subsurface structures and define the depth of upward penetration of the Pen Branch Fault in the Atlantic Coastal Plain (ACP) of South Carolina. In this environmentally sensitive area, determining the age of reactivation for this fault is important. Finding the shallowest flat lying layer can indicate the end of fault reactivation.

Typically in processing seismic data, refracted and reflected arrivals are separated. The acquisition and processing steps focus on one or the other but not both. This study entails the processing of refracted arrivals that are present in multifold reflection data as opposed to the use of single-fold data (Palmer, 1980). In conventional processing of reflection data set, the refracted arrivals are muted out to eliminate interference with the reflections. Utilization of the reflected arrivals requires the use of hyperbolic normal moveout that causes wavelet stretching and makes it difficult to image shallower structures with high resolution. In this study, refracted arrivals are stacked after linear moveout to image shallower structures. These structures are compared to the results with structures imaged by reflection processing done by Berkman, (1991), Sen (1991), Çoruh and Costain, (1994), and Domoracki, (1995). The basic processing steps used in generating the final refraction stack sections as given by Çoruh et al., (1993, 1995) are similar to those steps suggested for processing of reflected arrivals (Yilmaz, 1987).

In this study, refraction stack sections are generated from five high resolution reflection data sets originally acquired for reflected arrivals; they are PBF lines 6, 11, 12, 13, and 17. Shallower subsurface structures are imaged at about 4 - 18 m in depth from the surface to constrain possible shallow deformation across the Pen Branch Fault. Before discussing the seismic data sets and results from reprocessing, an overview of the geology of the study site is presented. Studies of Berkman, (1991), Sen, (1991), Cumbest and others, (1992), Fallow and

Price, (1992), Fallow and others, (1992), Snipes and others, (1992, 1993), Stieve and others, (1993, 1994), Coruh and Costain, (1994), and Domoracki, (1995) range from stratigraphy, structure, basin and fault development with the use of borehole log data, seismic reflection data, gravity and magnetic surveys; almost all targeted to better understand the Pen Branch Fault.

Geology

The extensive research that has been done in the area of the Pen Branch Fault is because of its location in the Savannah River site (Figure 1). The site is on unconsolidated to poorly consolidated ACP sediments of Late Cretaceous to Recent age over Triassic clastics and Paleozoic crystalline rock.

Dunbarton Basin

The Pen Branch Fault is identified as the northwest border fault of the Dunbarton Basin. Siple (1967) originally identified the Dunbarton Basin, a buried Mesozoic (Triassic) extension basin in the southeast part of the site. The Dunbarton Basin is 20 km east of the Riddleville Basin (buried Triassic basin in east central Georgia) and might be connected to this basin as being a northeast extension (Peterson et al., 1984). Daniels and others (1983) noted that the Dunbarton Basin has southeast dipping sediments, a northeast elongation, and a smaller thickness, while the Riddleville has northern dipping sediments, trends east-west, and has a greater thickness. They also pointed out that the Dunbarton Basin is the most southern basin and parallels the Appalachian tectonic trend. The PBF boreholes (Figure 2) provide a better constraint on the location of the northeast border of the Dunbarton Basin (Cumbest, et al., 1992). Boreholes PBF-2, PBF-5, PBF-6, PBF-7, PBF-8 contained clastic sediments that are associated with the Triassic basin, while boreholes PBF-1, PBF-3, PBF-4 to the north do not. The clastics of the Dunbarton Basin, originally below the top of the crystalline rocks, are about 24 - 30 m (80 - 100 ft) above the top of the crystalline rocks (Snipes et al., 1993). This is an indication of reactivation of the border faults. According to Domoracki (1995), the Dunbarton Basin is 15 km

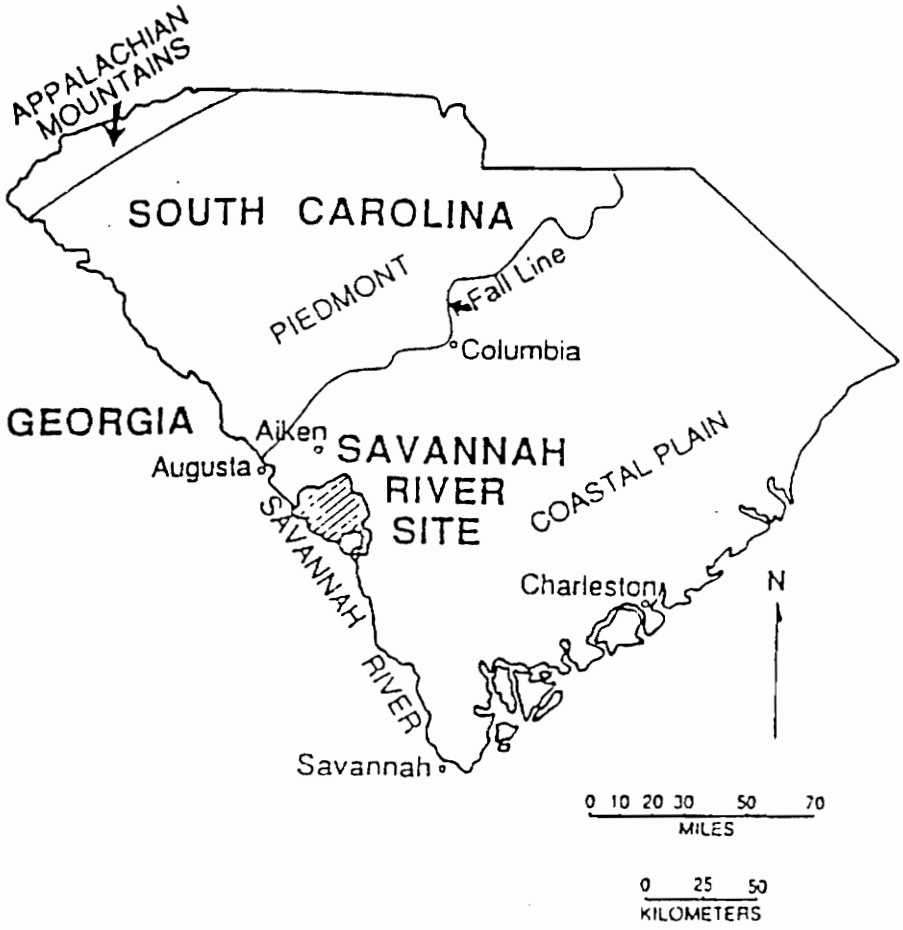

Figure 1. Savannah River site location map: (From Snipes et al., 1993)

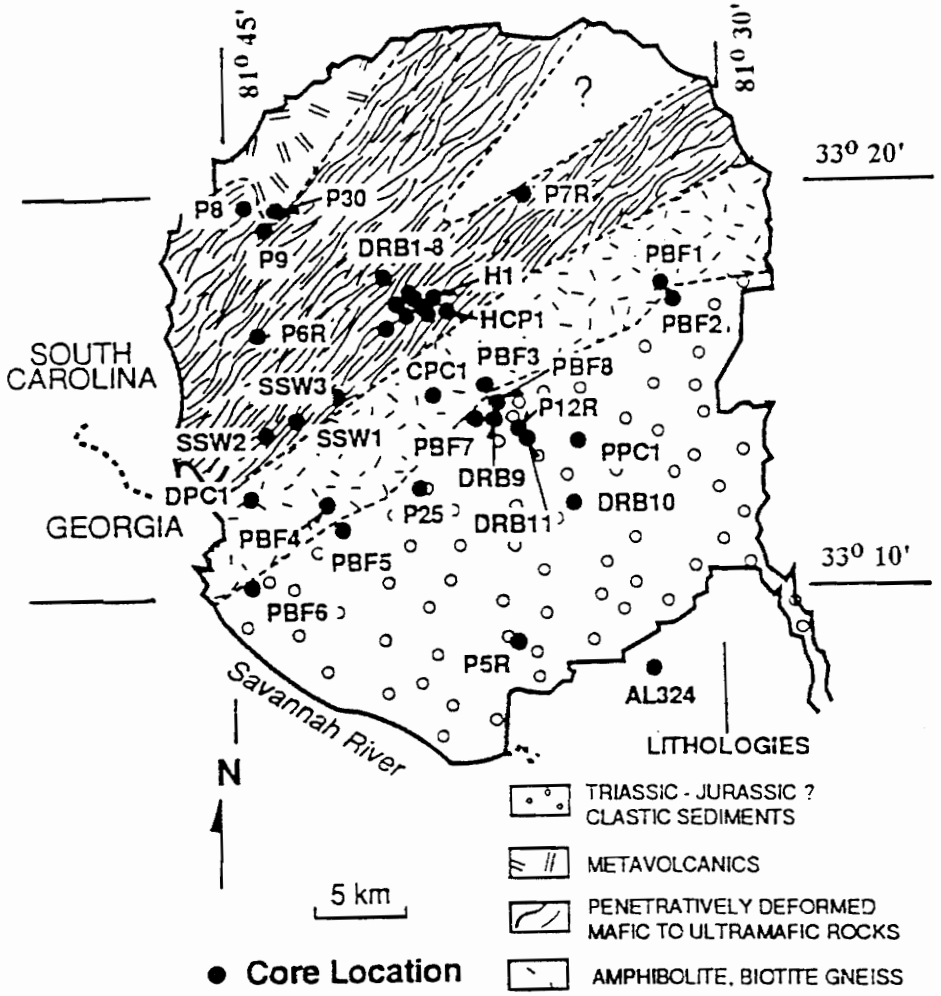

Figure 2. Savannah River Site basement geology map: (From Cumbest et al., 1992)

wide and at least 14 km long with synrift deposits and intrabasinal faults in the basin sediments. Postrift sediments might have been eroded or never deposited in the area.

Stratigraphy

The southeast dipping ACP sediments overlie crystalline rocks of Paleozoic age in the northwest part of the site. These sediments overlie Triassic clastics of the Dunbarton Basin with early Mesozoic fluvial deposits in the southeast (Snipes and others, 1993). According to Colquhoun and Muthig (1991), the depositional environments associated with these ACP sediments of the site area include upper delta plain, shallow siliclastic shelf and marginal marine. They further describe these three environments. First, the upper delta has a fluvial environment of point bars, channels and overbanks with medium to coarse, poorly to moderately sorted sands with clays and silts interbedding. Then, the shallow shelf is represented by fine to medium grain and moderately to well-sorted quartzitic sands with some silt, clays and limestones. Lastly, the marginal marine environment represents a tidal, beach and barrier environment with fine to medium grained, well sorted quartzitic sands with silts and clays. Berkman (1991) described sediments as sands, clayey sands, clays and some carbonates that represented fluvial, deltaic and near shore marine environments. He points out that the variability in the lithologies throughout the site might be caused by stream channels and meander belts. The site has tributaries associated with the Savannah River that is at the southwest border of the site.

Sediment thickness is 24 - 30 m (80 - 100 ft) at the base of the Late Cretaceous Cape Fear to 9 m (30 ft) at the top of the Late Eocene Dry Branch Formation (Snipes and others, 1992). An overview of part of the stratigraphy in the Savannah River Site is shown in Table 1. The Paleocene age Ellenton Formation with deltaic sediments (Fallow and others, 1992) has been broken into two formations, the Sawdust and the Lang Syne. The Sawdust (lower) is 3 m (10 ft) thick in the northwest and 12 m (40 ft) thick in the southeast, while the Lang Syne (upper) is scarce in the northwest and 24 m (80 ft) thick in the southeast (Fallow and Price, 1992). There are only a few cores available from the formation from the middle of the area (Fallow and others, 1992). The Late Paleocene or Early Eocene Snapp Formation, also of deltaic sediments, is 21 m (70 ft) thick near the southeast and pinches out at the Upper Three Runs in the northwest while the Early Eocene Fourmile Formation with shallow marine sediments is 10 m (30 ft) thick

Table 1. Stratigraphic Overview (based on Fallow and Price, 1992)

AGE	GROUP	FORMATIONS		LITHOLOGY DESCRIPTIONS
Miocene (?)		"Upland Unit"		Poorly-sorted, clayey and silty, fine to coarse sands; lenses and layers of gravels, pebbly sands and oxidized clays; clay clasts common
Late Eocene	Barnwell Group	Tobacco Road Sand		Red, tan, purple and orange, silty, clayey sands with some thin clays; flat quartz pebbles marks base in some places.
		Dry Branch Formation	Irwinton Sand Twiggs Clay Griffins Landing Members	Yellow, orange and tan, moderately sorted sand with interbedded clays; calcilutite, calcarenite, bioclastic limestone, calcareous sand, and shelly, calcareous clay
		Clinchfield Formation	Riggins Mill Utley Limestone Members	Tan, yellow, fine-coarse sand, poorly-well-sorted and; bioclastic, glauconitic limestone and calcareous sand and calcarenite
Mid Eocene	Orangebur Group	Tinker Creek Formation "Blue Bluff" Unit Santee Limestone		Sands, silts and clays, yellow, tan and white sand and pale green sands, clay beds and laminae; gray and pale green, clayey, laminated calcilutite and calcareous silts and clay with shelly layers and limestone lenses and some sand laminae
		Warley Hill Formation		Brown, green, tan, yellow and orange fine to medium, poorly to well-sorted sand and some glauconiti
Early Eocene		Congaree Formation		Orange, yellow, tan and greenish-gray, fine to coarse, moderately to well-sorted sand, some thin clay laminae
	Black Mingo Group	Fourmile Formation		Yellow, tan, orange. green and gray, fine to coarse, moderately to well sorted sand with green clays interbedded
Late Paleocene		Snapp Formation		Yellow, orange, tan, gray, medium to coarse sands interbedded with clay; generally poorly sorted sands, silty and micaceous sands.
		Lang Syne Formation		Lignitic, dark gray to black clays with micaceous, silty and clayey sands, pebbly sands with interbedded dark gray clays; glauconitic

in the northwest and overlies the Lang Syne and thins over top of the Snapp in the southeast (Fallow and Price, 1992). The lower part of the Congaree might be Early Eocene, and the upper part, Middle Eocene (Fallow and others, 1992). The Congaree contains shallow marine and barrier sediments and is 18 m (60 ft) thick at the northwest boundary and 24 m (80 ft) thick at the southeast boundary, while the Warley Hill with shallow marine sediments is difficult to determine because it is sporadic (Fallow and Price, 1992). The Warley Hill is present in the central part but not in the northwest. Unconformably overlying the Warley Hill is the Santee Limestone. Fallow and Price (1992) describe the Santee as mostly inner to middle neritic Middle Eocene sediments, 18 m (60 ft) thick in the center of the site. They go on to describe that the Santee is associated with three gradational units, which are the Santee Limestone, Blue Bluff and Tinker Creek. Continuing on with their description of the three units, the Santee grades to the southeast into the Blue Bluff that has sediments corresponding to the sediments of the McBean Formation. The Blue Bluff is 27 m (90 ft) thick at the southeast boundary and is associated with an environment that is of a lower energy than the Santee. The Tinker Creek ("green clay") has a southwest to northeast trend through the middle of the site and intertwines with the Santee and is 12 m (40 ft) thick at the northwest boundary. The sediments are associated with barrier, shallow marine and lagoonal environments. The Late Eocene sediments are 36 m (120 ft) thick in the center of the site and are associated with a shallow marine and lagoonal environment (Fallow and others, 1992). The Late Eocene contains the Barnwell Group that includes the Clinchfield Sand, Dry Branch Formation and the Tobacco Road Sand. This group unconformably overlies the Huber and Congaree Formations (Early Eocene) (Nystrom Jr. et al., 1991). The Huber Formation is composed of Paleocene and Early to Middle Eocene sediments deposited near the Fall Line and possibly includes age equivalents of the Warley Hill, Santee or McBean (Fallow and Price, 1992). The Utley Limestone of Clinchfield is not present in most of the site except possibly in channels, deposited on a shallow shelf environment (Harris and Zullo, 1992). The Clinchfield (Middle to Late Eocene) is about 9 m (30 ft) thick in the southeast and might either pinchout or becomes unrecognizable updip towards the center of the site (Fallow and Price, 1992). Unconformably overlying the Clinchfield is the Dry Branch that includes the Griffins Landing (mainly in the southeast with a thickness of about 21 m (70 ft) and possibly pinches out in the center of the site and grades into the Irwinton), Twiggs Clay and Irwinton Sand members, while the Tobacco Road Sand overlies the Dry Branch and is 15 m (50 ft) thick

in the middle of the site (Fallow and Price, 1992). The Tobacco Road Sand and the Dry Branch Formation are representative of a marginal marine environment (Harris and Zullo, 1992), with channeling of the Tobacco Road Sand (Fallow and others, 1992). The Upland unit, possibly of Miocene age, unconformably overlies the Barnwell group but in some instances overlies the Middle Eocene McBean Formation (Nystrom Jr. et al., 1991). The Upland unit is located at higher elevations at the site and is composed of fluvial deposits (Fallow and others, 1992).

Tectonic activity in the Cenozoic has included uplift, subsidence, and faulting (Prowell and Obermeier, 1991). The sediments of Georgia and the Carolinas have been altered since the Cretaceous by the Cape Fear Arch, the Charleston and Southeast Georgia Embayments. The Cape Fear Arch has affected the sediment thickness from the Late Cretaceous to the Tertiary (Nystrom Jr. et al., 1992). Uplift and subsidence have affected the coastal margin during Cretaceous and Cenozoic. Uplift in the Blue Ridge and Piedmont has caused fluvial deposits to come down and cover the upper ACP during the late Middle to early Late Miocene (Nystrom Jr. et al., 1992).

Pen Branch Fault

Reactivation of the basin normal faults has occurred during the Late Cretaceous (Chapman and Di Stefano, 1989). The Pen Branch Fault is interpreted to be a reactivated border fault of the Dunbarton Basin in the northwest (Snipes et al., 1993). This 80° to vertical dipping fault has Late Cretaceous sediment that is 203 m (670 ft) thick on the downthrown side and 185 m (610 ft) thick on the upthrown side with its throw decreasing as the sediments get younger (Snipes et al., 1992). The Late Cretaceous to Tertiary fault is also considered to be a growth fault, with down to the northwest movement, with an average strike of N55°E, and an average rate of slip 0.4 m/ m.y. over last 85 my (Snipes et al., 1993).

Previous Studies

Recent studies on the Pen Branch Fault and surrounding area (Figure 3) based on seismic and borehole log data that are included in this study of refraction stacks are Berkman (1991), Sen (1991), Snipes and others (1992,1993), Stieve and others (1994a, b), Çoruh and Costain (1994)

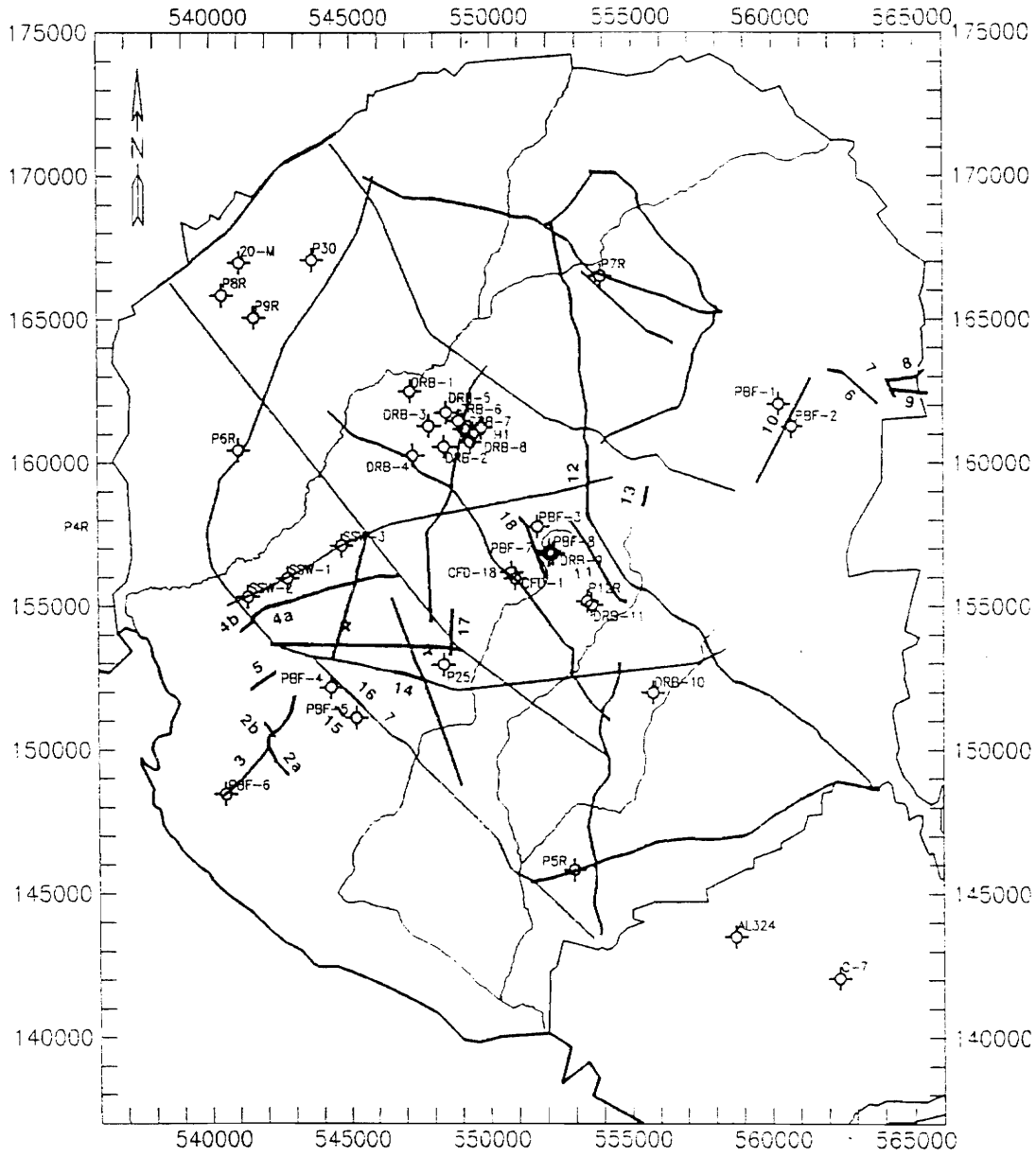

Figure 3. Seismic lines and boreholes location map: Map showing the high resolution PBF lines (numbered), the SRS lines and the boreholes (labeled). The South Carolina state grid coordinates are given in meters. (From Çoruh and Costain, 1994).

and Domoracki (1995). The Pen Branch Fault is the main through going fault in the site. Finding the age of reactivation of this fault and others is considered important because of a seismic threat. A brief summary of the previous studies is given below.

Berkman (1991) reports his interpretation of the PBF high resolution seismic and borehole data. Berkman interprets interfaces of sand and clay with stream channels and meander belts. He suggests that the Pen Branch Fault breaks only to the Cape Fear Formation and there is some deformation of overlying units.

Sen (1991), using Conoco SRS vibroseis reflection data sets and a PBF high resolution data set (PBF line 6), studies the removal of near-surface effects to better constrain the upward penetration depth of the Pen Branch Fault. Sen reports the maximum offset of the Pen Branch fault at the basement level is about 32 m. The fault is projected up to about 0.15 s (two-way traveltime) (106 m) below the surface and associated antithetic faults up to about 0.16s (113 m) below the surface. Refraction stacks of the split spread data with muting are used to image subsurface structures. Shallower reflections between the surface and 0.25 s (180 m) below are of poorer quality for most of the lines.

Snipes and others (1993) use boreholes and the Conoco SRS vibroseis reflection data. The Pen Branch Fault is interpreted to project upwards as shallow as the Dry Branch Formation (Late Eocene), where a 9 m (30 ft) offset is observed. Seismic sections of the upper 0.5 s show the ACP sediments. They interpreted an offset up through the lower Late Eocene unit while no offset at the Quaternary soil above.

Çoruh and Costain (1994) reprocess the PBF high resolution reflection data along with correlations with the PBF borehole log data, originally processed by Berkman (1991), to attempt determining the shallowest flat lying layer to constrain upward penetration of the Pen Branch. Clearer deformations and offsets are determined from PBF lines 6, 13, 17, and 18. Some of the lines have reflectors resolved as shallow as 20 - 30 ms (two-way traveltime), from the surface. An opposite sense of motion is interpreted in the far southwest part of the site between PBF lines 3 and 15 (Figure 3), then there is an area with zero offset between these two lines.

Stieve and others (1993) have prepared cross sections (created from borehole logs and lithology correlations) that shows the base of Tobacco Road Sand around 15 m (50 ft) deep and in some places the base of the Upland unit to be around 9 - 12 m (30 - 40 ft). The CFD boreholes from the Confirmatory Drilling Project are located near the center of the site near PBF

line 18. Stieve and others (1994 a, b) detail the drilling project where CFD boreholes are placed along part of the fault zone to determine the presence of any flat laying layers that can cap off the Pen Branch Fault. Analysis of CFD and geophysical data constrains the limit in deformation of sediments below the Upland unit. It is observed that the Tobacco Road Sand might be the shallowest layer that is mappable with its base affected by deformation and might cap off the Pen Branch Fault because the Upland unit is typically unrecognizable (Stieve et al., 1994a). The deformation might be as far up as into the Dry Branch Formation and be related to primary deposition features than to a fault because strain cannot be reasonably measured or traced above the Williamsburg Formation (Stieve et al., 1994b). The sediments of the Williamsburg correspond to those of the Snapp Formation and these upper Paleocene and lower Eocene sediments overlie the Ellenton downdip (Fallow and others, 1992).

Domoracki (1995) has reprocessed all available seismic data over the Dunbarton Basin and the rest of the site and reported on basement structures and the upward extent of faults into the ACP sediments. Interpretation is based on reflection seismic sections using mainly the Conoco SRS vibroseis reflection data. Time-structure and reflection amplitude maps are generated from the data. Five major reflection events were interpreted by Domoracki (1995): the basement is interpreted to be at a depth of 300 - 320 m (91 - 98 ft). Other reflections were interpreted to be from the top of the Cape Fear Formation (the green marker of Domoracki), the top of the Middendorf or base of the Black Creek, Late Cretaceous (blue marker), and the middle Black Creek Formation (orange marker). The shallowest event resolved was interpreted as the top of the Late Cretaceous Peedee Formation or the base of Early Paleocene Ellenton Formation (yellow marker). Both the blue and yellow markers are affected by the Pen Branch Fault, which offsets these horizons. The blue marker is interpreted 65 to 115 ms above the basement and the yellow marker is 160 to 125 ms above. The displacement on the fault is described here as being approximately 30 m (100 ft) at the top of the basement. In Domoracki (1995), the Pen Branch Fault is part of 3 km fault zone that also includes subparallel faults of smaller throws and locally developed splays. The Pen Branch Fault is a reverse fault that dips to the southeast. The subparallel faults usually have down-to-the-northwest movement north of the Pen Branch Fault or down-to-the-southeast movement south of the fault. He goes on to say that movement through the Late Cretaceous was accompanied by tilting and rotation of blocks. The rotation has changed the strike of the Pen Branch Fault from N55°E to N70°E in the northeast section of the site near

PBF line 6. The average slip is calculated as 0.22 m/my as supposed to an average 0.4 m/my in Snipes and others (1993). Domoracki points out that other basement faults in South Carolina that are reactivated have deformation affecting the topography. Erosion might have been a cause for the absence of deformation at the surface that might have been associated with the Pen Branch Fault. There has not been conclusive evidence of deformation associated with the Pen Branch Fault at the ground surface in the site.

All the major results in mind, in this study, the refraction stack sections (Çoruh and others, 1995) on selected PBF lines across the Pen Branch Fault are generated to constrain the deformation of the fault between the surface and yellow horizon of Domoracki at about 0.14 s (about 100 m). The refracted arrivals exhibit possible deformation as shallow as 4 m.

Seismic Data

The PBF high resolution reflection data set originally processed by Berkman (1991) was recorded by ESI Geophysical, Inc. in subcontract with Emerald Exploration Consultants, Inc. under contract with Westinghouse Savannah River Co. The data package included 17 short lines across the projected Pen Branch Fault zone (Figure 4). Results from the original data processing were given by Berkman (1991). The same data package was later reprocessed at the Regional Geophysics Laboratory of Virginia Tech. Results from this processing were given by Çoruh and Costain (1994). During Virginia Tech processing, use of refracted arrivals was tested to better image shallow structures and encouraging results of the test refraction stack sections led to this study in which PBF lines 6, 11, 12, 13 and 17 were used to map shallower deformation using the refraction stack sections.

The recording of these lines was done with E G and G Geometrics ES-2401 24-channel recording seismograph using a buffalo gun energy source. The spread was an asymmetric split spread with stations every 6.1 m (20 ft) and shots at every half station at 3 m (10 ft) spacing. A recording filter of 50 - 1000 Hz with a 60 Hz notch was used. These parameters were used for the five PBF lines except for line 17, where the near trace offset of 90 m (295 ft) and a filter of 70 - 1000 Hz were used. The PBF line 17 line was designed to record deeper in the reflections. A summary of parameters for the processed lines is has been given in Table 2. The SRS Conoco lines were used to help constrain the location of the Pen Branch Fault at depth and to correlate it with the shallow deformation mapped in the PBF lines. The reflection stack of PBF line 6 and part of the reflection stack of SRS line 3 from Domoracki (1995) were included in figures in this study while the other processed lines were just referenced.

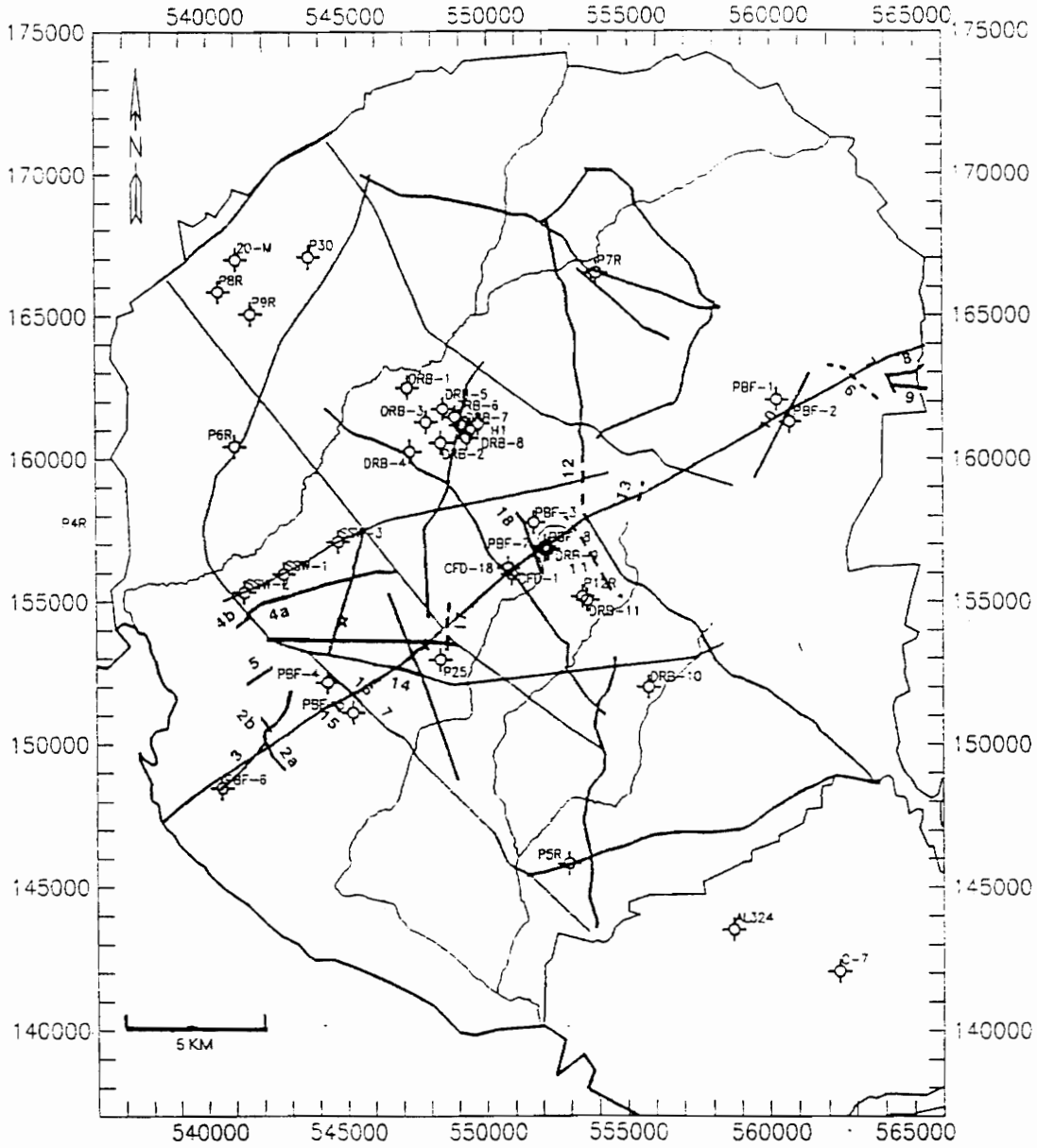

Figure 4. Seismic lines and boreholes location map: Map showing the high resolution PBF lines (numbered), the SRS lines and the boreholes (labeled) along the approximate location of the Pen Branch Fault. The dashed lines are the PBF lines used in this study. The South Carolina state grid coordinates are given in meters. (Altered from Çoruh and Costain, 1994).

Table 2. Recording Parameters of the Processed Pen Branch Fault High Resolution Seismic Lines

Line Number	PBF 6	PBF 13	PBF 12	PBF 11	PBF 17
Station Range	101-467	101-245	101-501	101-690	101-371
Line Length (km)	2.2	0.7	2.4	3.5	1.6
Near-Far Offset (m)	18-6-0-6-120 21-9-0-3-117	18-6-0-6-120 21-9-0-3-117	18-6-0-6-120 21-9-0-3-117	18-6-0-6-120 21-9-0-3-117	0-90-222 0-87-219
Group Interval (m)	6.1	6.1	6.1	6.1	6.1
Shot Interval (m)	3	3	3	3	3
CMP Fold	12	12	12	12	12
Source	Buffalo Gun 90 gr. load	Buffalo Gun 90 gr. load	Buffalo Gun 90 gr. load	Buffalo Gun 90 gr. load	Buffalo Gun 115 gr. load
Receiver Array	6 geophones potted on flag	6 geophones potted on flag	6 geophones potted on flag	6 geophones potted on flag	6 geophones potted on flag
Original Sample Rate (ms)	0.2	0.2	0.2	0.2	0.2
Processing Sample Rate (ms)	1.0	1.0	1.0	1.0	1.0
Record Length (ms)	409	409	409	409	409

Processing of Seismic Data

Reprocessing was carried out to generate refraction stack sections following the flow chart given in Table 3. The steps and concepts used to process the seismic data were those generally used in reflection processing, except that, because refracted arrivals were the emphasis here, no first arrival muting was used and the moveout was linear instead of hyperbolic. The reprocessing was done on a VAX 11/785 and Sun Sparc workstations using CogniSeis' DISCO and FOCUS processing packages and software modules such as REFSTK (stacking for refracted arrivals) developed in the Regional Geophysics Laboratory.

Data Preparation

The geometries of the lines were already available because the PBF high resolution data sets were previously reprocessed at Virginia Tech. During the line geometry preparation the number of stations was doubled to accommodate energy sources between receiver stations. For final display the station numbers were renumbered back to the original values. The data were resampled from 0.2 ms to 1.0 ms. An AGC with a 200 ms window and a bandpass filter of 60-70-200-220 Hz were applied.

Datum Statics

After preliminary testing for calculating datum statics corrections (more details in the Appendix), it was decided to use the corrections based on the elevation static correction with a constant datum velocity of 900 m/s. The datum elevation used in calculation of the corrections was chosen to approximate the surface topography at each line location. The datum corrections were applied to the data that were sorted by common midpoint and offset as the major and minor keys, respectively.

Table 3. Reprocessing steps for the refraction stack sections for PBF lines

Resample from 0.2 to 1.0 ms
Edit traces
Amplitude balancing with AGC
Bandpass filter (first filter)
    60-70-200-220 Hz
Edit traces
Datum statics
Surface consistent residual statics (computed using reflected and refracted arrivals)
CMP sort
Velocity analysis with linear refraction moveout
Collect adjacent CMPs
Amplitude balancing with AGC
Refraction stacking
Predictive deconvolution
    8 ms gap
    50 ms operator length
    0 - 100 ms design gate
    0 - 200 ms application gate
Bandpass filter (second filter)
    Low freq. cutoff: 80 Hz
    High freq. cutoff: 220Hz
    Slope: 6 dB/cycle
Amplitude balancing with AGC
Signal
Digistk
Amplitude balancing with AGC
Display

Refraction Velocity Analysis

Constant velocity panels based on linear refraction moveout corrections were used to determine refraction stacking velocities. A group of CMPs was conventionally stacked after the refraction velocity moveout correction is applied using trial velocities using the DISCO module RVMO. The main criteria were to pick the velocity that resulted in a high signal to noise ratio with the best wavelet shape. On PBF lines 6 and 13 the refraction velocity analysis was done only after applying available residual statics from reflection processing. For the other lines preliminary velocity analyses were carried out first for use in surface consistent residual statics. Final stacking velocities were determined from a second velocity analysis after applying the residual statics computed from refracted arrivals. For determining of the stacking velocities for the refraction stacks, adjacent common mid-point gathers were collected from about every 50 consecutive gathers along each line and were stacked. Constant velocity panels were created using about 12.5 stations and corresponding velocities were picked. Examples of velocity panels were given along with the final refraction stacks for verification. The location of the example panels has been indicated by "V" in the final refraction interpretation stack sections. The location of the other velocity panels not included in the examples has been indicated by a point (". "). Figure 5 has shown a CMP gather before and after refraction moveout correction and the data after stacking for the refracted arrivals. The processing flow included predictive deconvolution after stack along with filtering and amplitude balancing after the deconvolution.

Residual Statics

For PBF 6 and PBF 13 available statics from the reflection reprocessing were applied. For the other lines, the residual statics were computed, using STATICR DISCO module with a maximum 3 ms allowable shift in a four-iteration scheme, from the refracted arrivals after linear moveout was applied. Seven CMPs were summed to obtain the pilot trace for correlation within STATICR. Two passes of four-iteration statics were applied on these PBF data sets to generate the refraction stack sections.

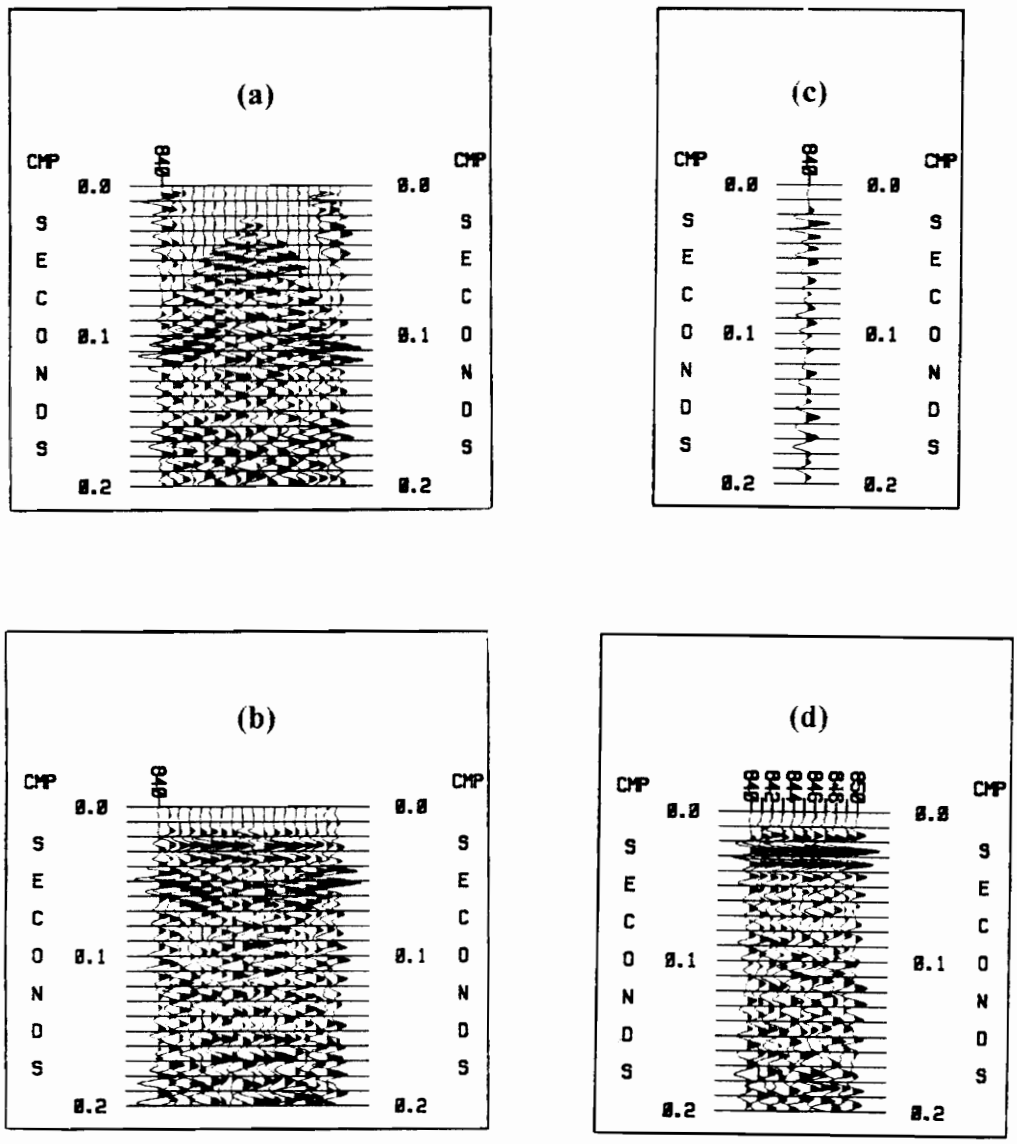

Figure 5. Example of a refraction stack: The CMP 840 gather from PBF line 13 is shown in (a) before refraction moveout correction, (b) after refraction moveout correction using a velocity of 1650 m/s, and (c) after stacking the data in (b). (d) shows traces stacked from CMP 840 - 850.

Refraction Stack

Conventional use of refraction arrivals usually entailed single fold data with use of forward and reverse travel times as in the general reciprocal method (GRM) of Palmer (1980), where a velocity analysis function and a generalized time-depth function were determined. Instead of finding the exact location on the refractor where the forward and reverse raypaths emerge, a midpoint between geophone distances for the forward and reverse paths was used and the distance between these two points was optimum when the raypaths come from near the same refractor point (Palmer, 1981). This optimum distance was used to determine average velocities and time-depths to image the subsurface.

The refraction stack of Çoruh and others (1993, 1995) was designed to produce seismic refraction stack sections based on refraction delay time concept as most of the refraction methods have their origin. Çoruh and others (1993) set up the basis for the refraction stack assuming a horizontal refractor and using split-spread data, but the concept can apply to off-end data as well when the data was used in the CMP domain. Using Figure 6a, the traveltime path from source to receiver, the arrival time, was given by

$$t_x = t_0 + \frac{x}{v_2} \tag{1}$$

or

$$t_x = \frac{2h}{v_1}\cos i_c + \frac{x}{v_2}, \tag{2}$$

where $\frac{2h}{v_1}\cos i_c$ was the delay time and $\frac{x}{v_2}$ was the linear refraction moveout. The h was the layer thickness, v_1 and v_2 were the first and second layer velocities, and i_c was the angle of incidence. Also,

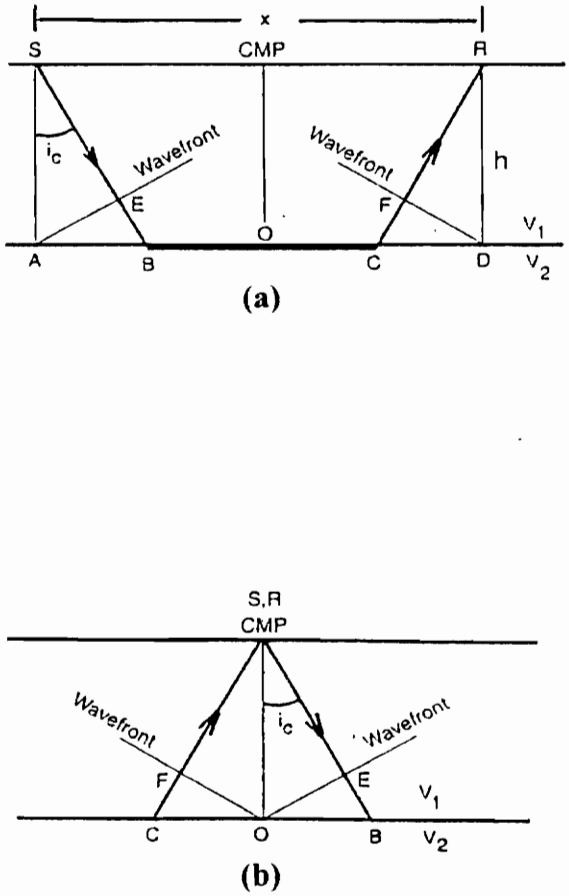

Figure 6. Critically refracted raypath before and after refraction moveout correction: (a) Critically refracted wave arrival for a horizontal layer is shown before refraction moveout correction. The CMP is the midpoint between the source and receiver. (b) Critically refracted wave arrival is shown after refraction moveout correction. The source and receiver are mathmatically moved to the CMP point. (From Çoruh et al., 1993)

$$\cos i_c = \sqrt{1 - \left[\frac{v_1}{v_2}\right]^2} \quad . \tag{3}$$

The linear refraction moveout was removed to convert arrival times of the refracted waves into delay times to simulate two-way reflection times. Removing the linear refraction moveout was similar to setting distance x equal to zero (zero offset), and the source and receiver were mathematically migrated to the same position, the common midpoint (CMP) (Figure 6b). Multifold reflection data had refracted raypaths that should cover a common area on the refractor. The midpoint of this area should correspond to a common midpoint. If the data were sorted by CMP, ensembles could be produced with common refractor surfaces (CRS) beneath a CMP (Figure 7a). The sorted CRS ensembles had arrival times with linear delay. The removal of the linear delay or refraction moveout reduced the wavelet onset times to a common delay time that simulated a source-receiver distance equal to zero (Figure 7b). The removal was performed using velocities obtained from the constant velocity analysis. The CRS ensembles, after the refraction moveout correction had been applied, were used as input to the refraction stacking program (REFSTK). The velocity would have been the refractor velocity, $v_2 = \frac{v_1}{\sin i_c}$, when the refractor was horizontal. If the refractor was not horizontal then the common delay time represented an average delay time. In the shot domain for the dipping refractor and off-end data the refraction stacking velocity would approximate the down-dip apparent velocity, $\frac{v_1}{\sin(i_c + \alpha)}$ (α was the slope angle), or the up-dip apparent velocity, $\frac{v_1}{\sin(i_c - \alpha)}$, depending on the direction of recording. The apparent velocity was lower than the true refractor velocity when down-dip and greater than the true refractor velocity when up-dip (Palmer, 1986). For split-spread data, the average of the down-dip and up-dip velocities was used for the apparent velocity. When the refractor was horizontal, the CMP of the data sets might have been attributed to the point directly below on the refractor, but in case of dipping refractor the projected point on the refractor was not directly (vertically) beneath the CMP, which could cause a smearing affect in addition to stacking data that represent a common refractor area (CRS).

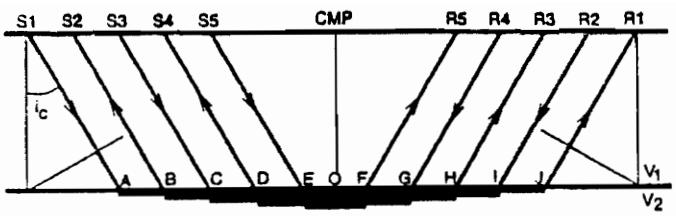

(a)

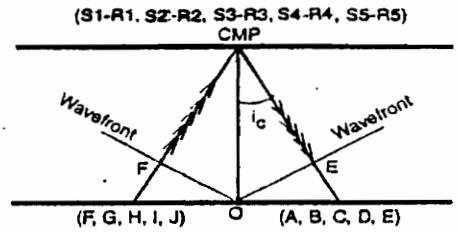

(b)

Figure 7. Multifold critically refracted raypath before and after refraction moveout correction: (a) Multifold off-end data sorted by midpoints forming a common refractor surface raypaths for a horizontal layer with maximum folding under the CMP point. (b) Raypaths are moved to the CMP point to represent refraction moveout correction. (Modified from Çoruh et al., 1993.)

Çoruh and others (1995) discussed the dipping refractor case in the common midpoint domain and revisited the refraction stack processing and determining delay time. They showed that apparent refraction stacking velocities were equal on direct and reverse profiles in the CMP domain. The apparent velocity was given by $\frac{v_2}{\cos\alpha}$. Using a sloping refractor (Figure 8), the arrival time of a critically refracted arrival between source and receiver was given by

$$t_x = \frac{x\cos\alpha}{v_2} + \frac{h_1 + h_2}{v_1}\cos i_c, \tag{4}$$

where h_1 and h_2 were the shortest distances from the source and the receiver to the refractor, respectively. If h_0 was the shortest distance between the refractor and CMP, then the distances h_1, h_2 and h_0 (Figure 8) had the following relations in the CMP domain, independent of recording direction:

$$\begin{aligned} h_1 &= h_0 - dh \\ h_2 &= h_0 + dh \\ h_1 + h_2 &= 2h_0. \end{aligned} \tag{5}$$

The dh was the difference between distances h_1 and h_0 or h_2 and h_0. From these relations, arrival time of critically refracted waves in the CMP domain could have been given as

$$t_x = \frac{x\cos\alpha}{v_2} + \frac{2h_0}{v_1}\cos i_c. \tag{6}$$

Therefore, velocity obtained from linear moveout constant velocity panels would indicate the apparent velocity, $\frac{v_2}{\cos\alpha}$, which could be used to remove the refraction moveout or linear delay, the time associated with the path between A and D or between E and F (Figure 8).

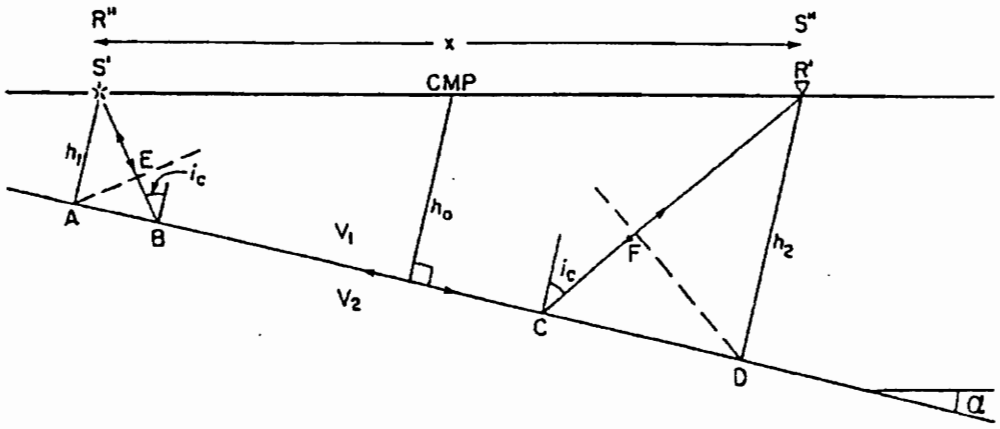

Figure 8. Critically refracted raypath for a sloping layer: The refracted arrival time can be changed to a delay time that represents the thickness under the CMP point. (Çoruh et al., 1995.)

The multifold reflection data were sorted with common midpoint and offset keys to create gathers that could be considered CRS ensembles for refracted arrivals. After removal of refraction moveout using the apparent velocity determined from velocity analysis, the corrected ensembles were stacked to create a refraction stack in the (CMP, t_0) domain. Amplitude balancing with an AGC of 100 ms was applied this time after stacking.

Deconvolution

Predictive deconvolution after refraction stacking was used to remove wavelet reverberations in the data (Figure 9). A gap of 8 ms and a filter operator of 50 ms were used for all the lines. This deconvolution was applied to the constant velocity analysis stacks for determining the stacking velocities and the final refraction stacks for subsurface imaging. The deconvolution was followed by a bandpass filter (second stage) and amplitude balancing, which are given below.

Filtering

The first filter used on the data sets was in the data preparation stage, with a bandpass filter (DISCO FILTER BAND option) with four frequency points (60-70-200-220 Hz). During the second stage of filtering, a bandpass filter (DISCO FILTER BANDSL option), with two frequency points and slopes, were used. The data in the first 100 ms was filtered using a low frequency cutoff of 80 Hz and a high frequency cutoff of 220 Hz with slopes of 6 dB/cycle. Filtering was followed by amplitude balancing with an AGC of 100 ms

Display

As an optional feature, a step (DISCO DIGISTK) was used to improve the continuity of the refraction stacks. Signal traces were derived from coherency estimations in a specified window and a maximum and minimum dip range . The window was 5 traces by 20 ms and incremented horizontally by one trace and vertically 5 ms. The signal traces were combined with the original data traces for enhancement using a 50% mix. The result was a slight increase in the

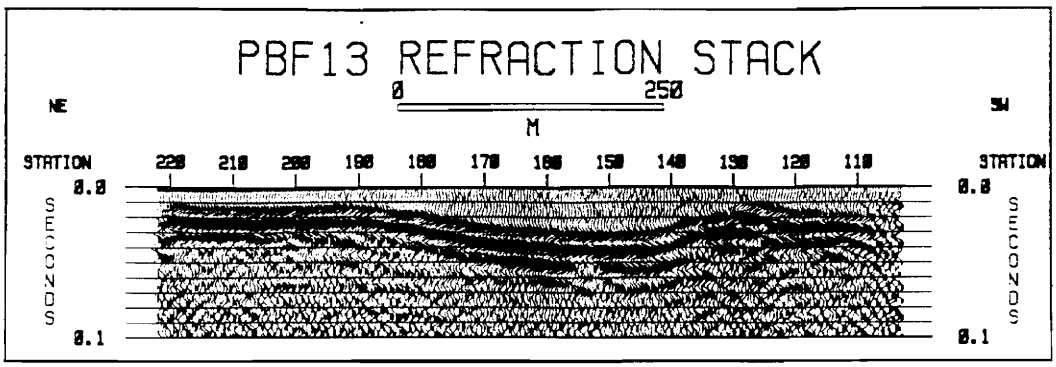

(a)

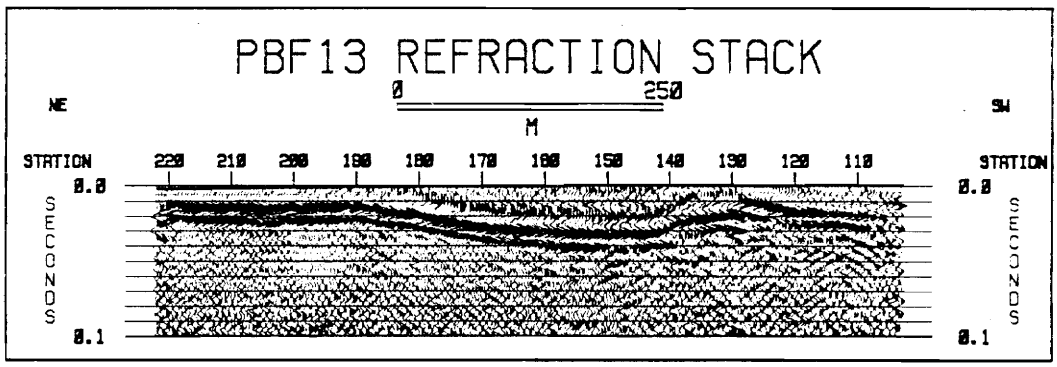

(b)

Figure 9. PBF line 13 refraction stack: (a) before a predictive deconvolution and (b) after a predictive deconvolution. A filter and amplitude balancing with AGC were applied to both (a) and (b).

continuity (Figure 10). The final refraction stack sections were displayed using the variable area only option to emphasize the amplitude peaks for interpretation (Figure 11b). However, for comparison with reflection stack sections the variable area with wiggle trace option is used (Figure 11a).

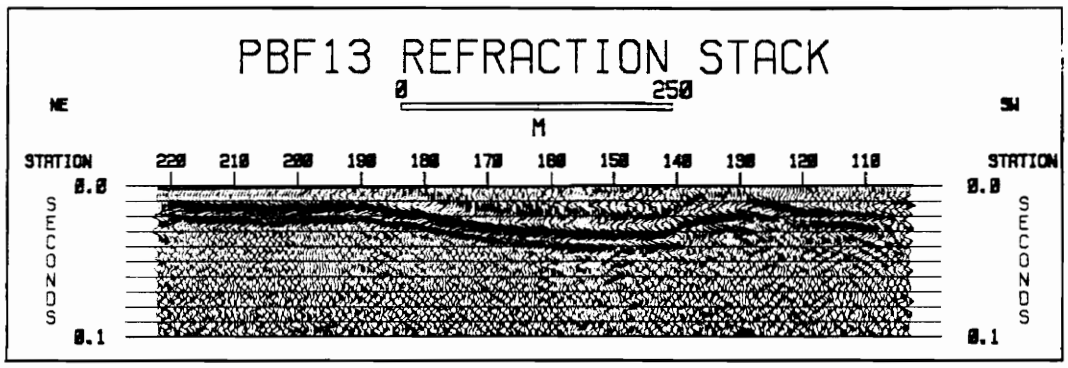

(a)

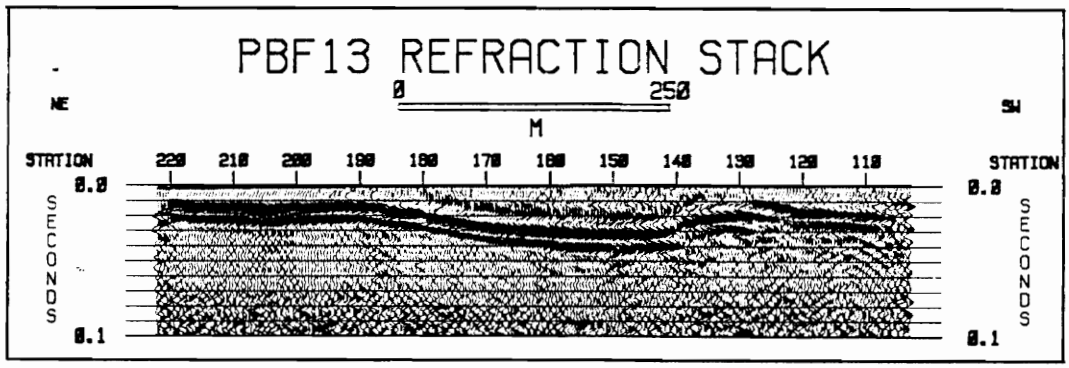

(b)

Figure 10. PBF line 13 refraction stack: (a) before DIGISTK and (b) after DIGISTK. Filter and amplitude balancing with AGC were applied to both (a) and (b).

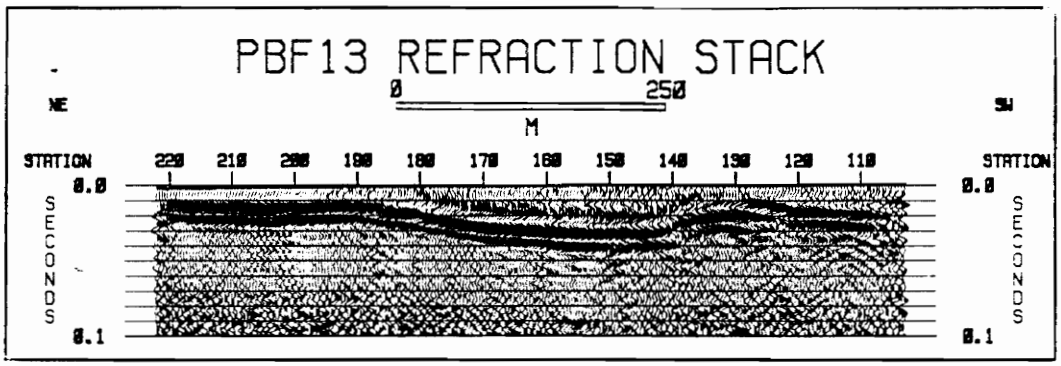

(a)

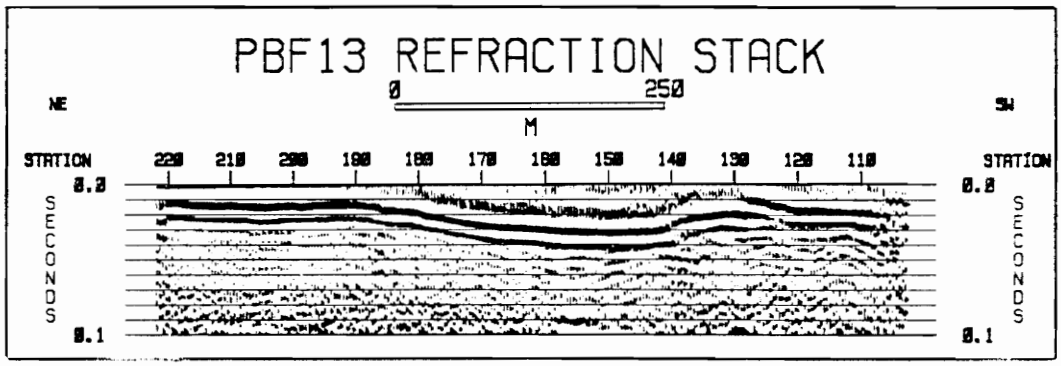

(b)

Figure 11. PBF line 13 final refraction stack: Displayed with (a) variable area with wiggle trace and (b) variable area only.

Results and Interpretations

The following are descriptions and interpretations of the results of the refraction stack sections generated from five PBF lines starting with PBF line 6 in the northeast ending with PBF line 17 in the southwest along the Pen Branch Fault zone (Figure 4). The shallowest depths affected by the Pen Branch Fault are in the northeast along PBF lines 6 and 13.

PBF line 6

The reprocessed portion of this northwest to southeast trending PBF line 6 (Figure 4) is between stations 200 - 350 and is about 0.8 km in length. The refraction stack with 80 m datum is created using a velocity range of 1500 - 1600 m/s for the first refractor (A) and 2000 - 2200 m/s for the second refractor (B) and the results are shown in Figure 12. Examples of the constant velocity panels and the final stacking velocities (indicated by V) are in Figures 13 and 14. The PBF line 6 is suitable to recover refracted events from deeper refractors, too. There is an offset interpreted between stations 275 - 280 on the second refractor (B), which might extend upwards into the first refractor (A) near station 275 (Figure 12). Another possible offset or deformation occurs beneath station 270 in the second refractor (B) and between stations 260 - 265 in the first refractor (A) causing an upwarp and/or offset. There are dipping features between stations 220 - 270 in first refractor (A) and between stations 200 - 270 in the second refractor (B), which might be stream channels or deformation caused by the possible fault area. The refractors do not seem to dip in the regional southeast direction of the ACP sediments. Using a velocity of 800 m/s (based on the constant velocity panels in Figure 15), the depths to the first refractor (A) are 8.0 m (station 200), 8.4 m (station 220), 11.2 m (station 240), 10.8 m (station 260), 8.0 m (station 270), 4.0 m (station 320), 4.0 m (station 350), and 8.4 m (station 360). The depths to the second

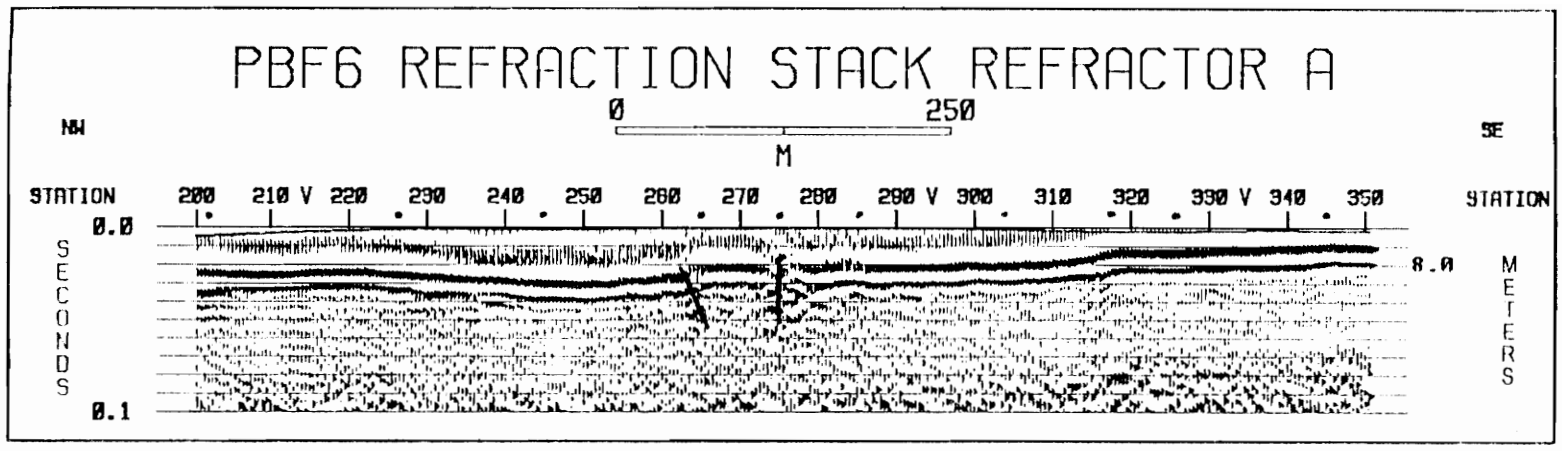

(a)

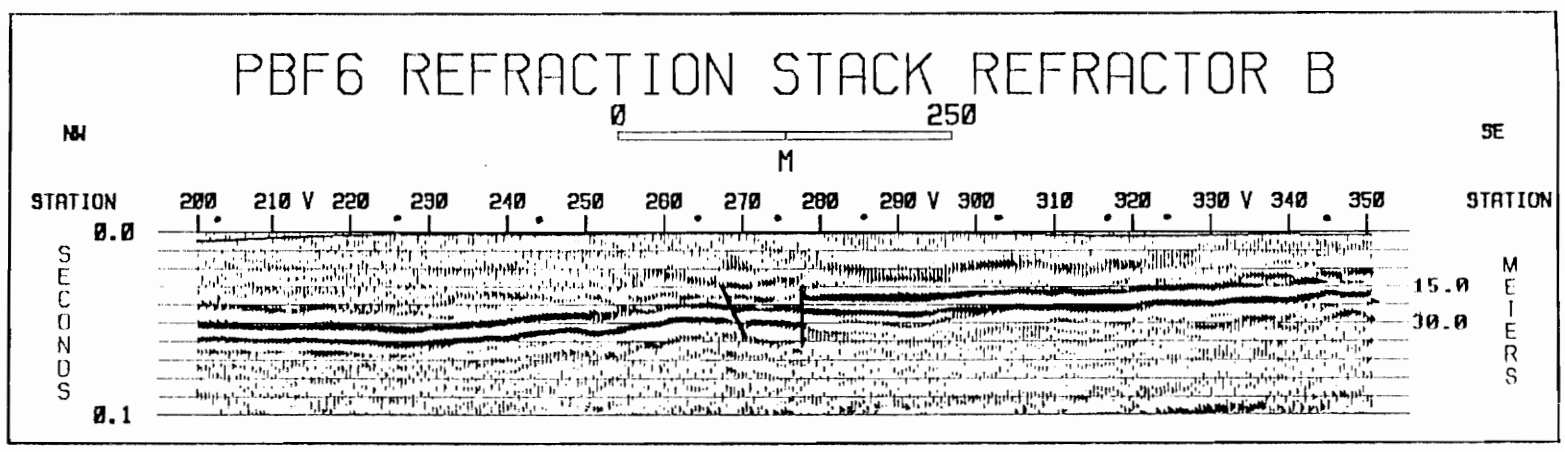

(b)

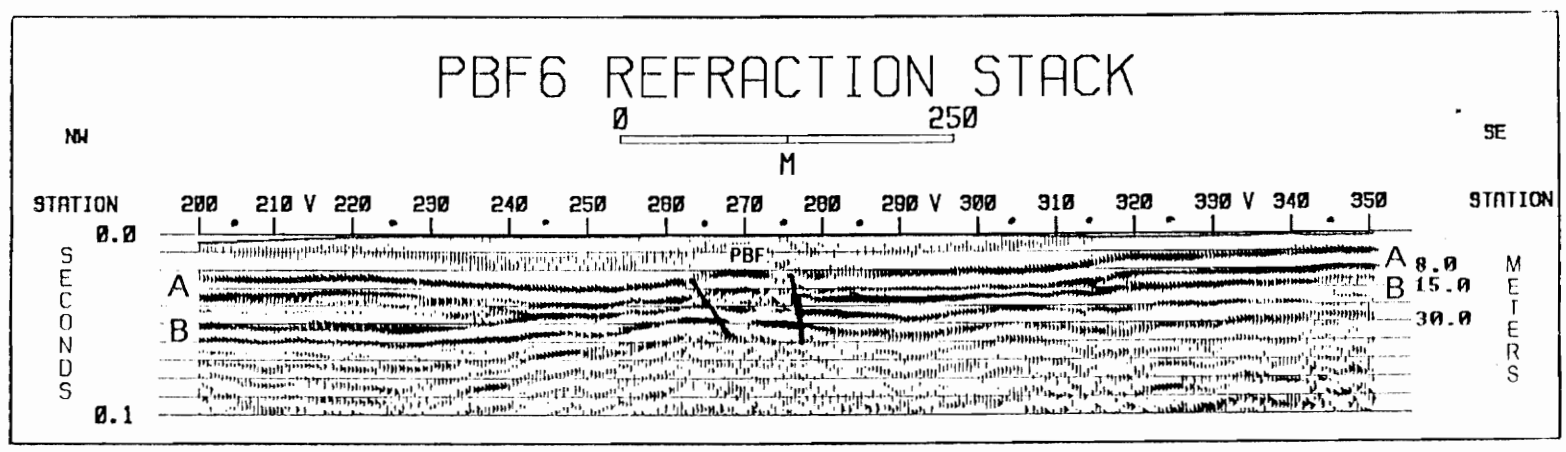

(c)

Figure 12. PBF line 6 refraction stacks: (a) The refraction stack created with a 80 m datum and a velocity range of 1500-1600 m/s. (b) The refraction stack created with a 80 m datum and a velocity range of 2000 -2200. (c) Composite refraction stack section created with time variant velocity functions to accommodate velocities from (a) and (b). V marks the area of stations used in the examples of the velocity analysis panels for determining stacking velocities shown in Figures 13 and 14. A point (•) marks the location of the other stations not included in the examples of the velocity analysis panels. Possible offsets are shown in the Pen Branch Fault zone. PBF = Pen Branch Fault.

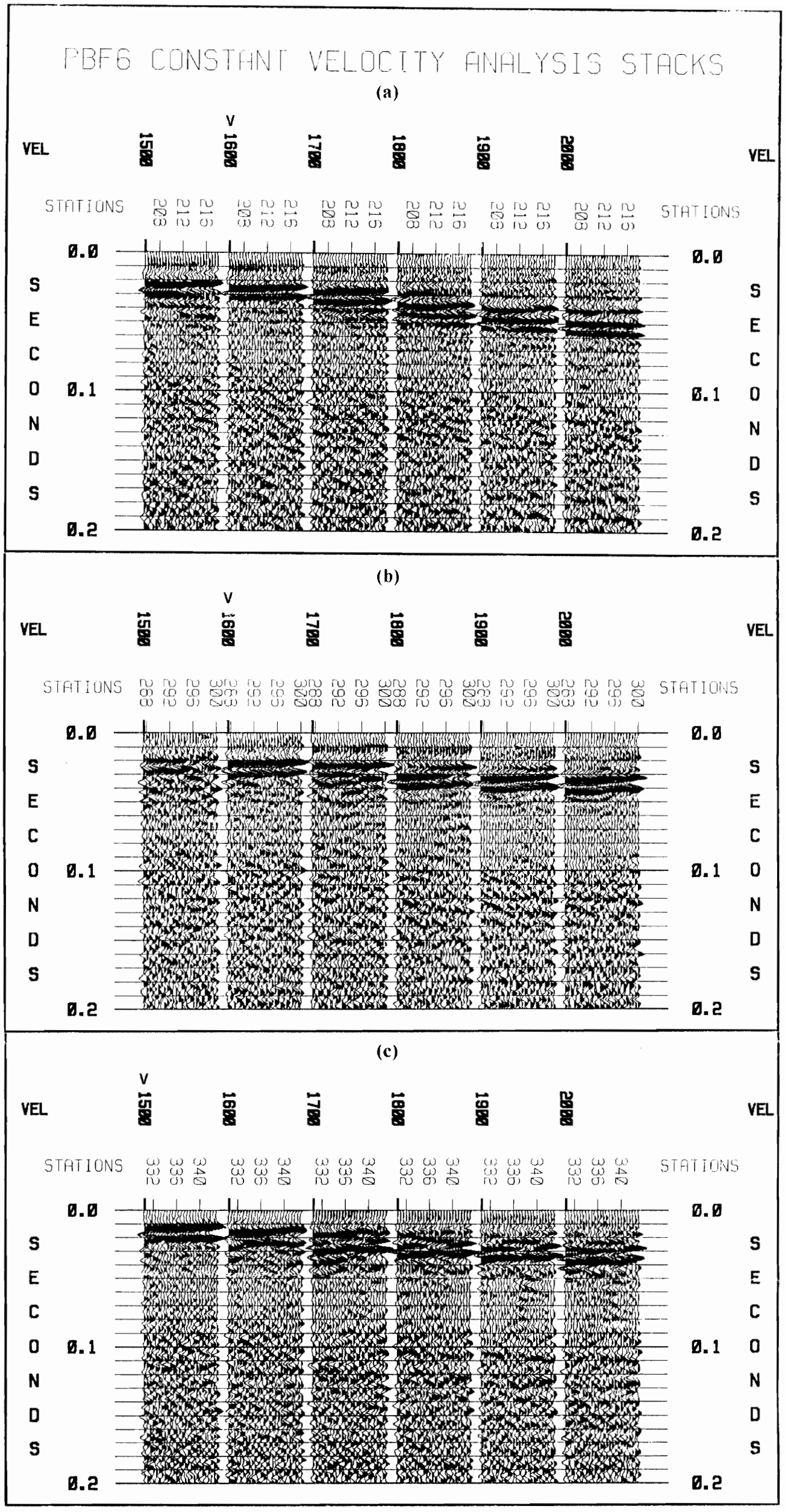

Figure 13. PBF line 6 constant velocity analysis panels for refractor A: Determination of refraction velocities at different station groups. Examples of some of the panels used are shown for (a) stations 205-218, (b) stations 287-300 and (c) stations 330-343. V marks the velocity chosen for the refraction stack from that station group.

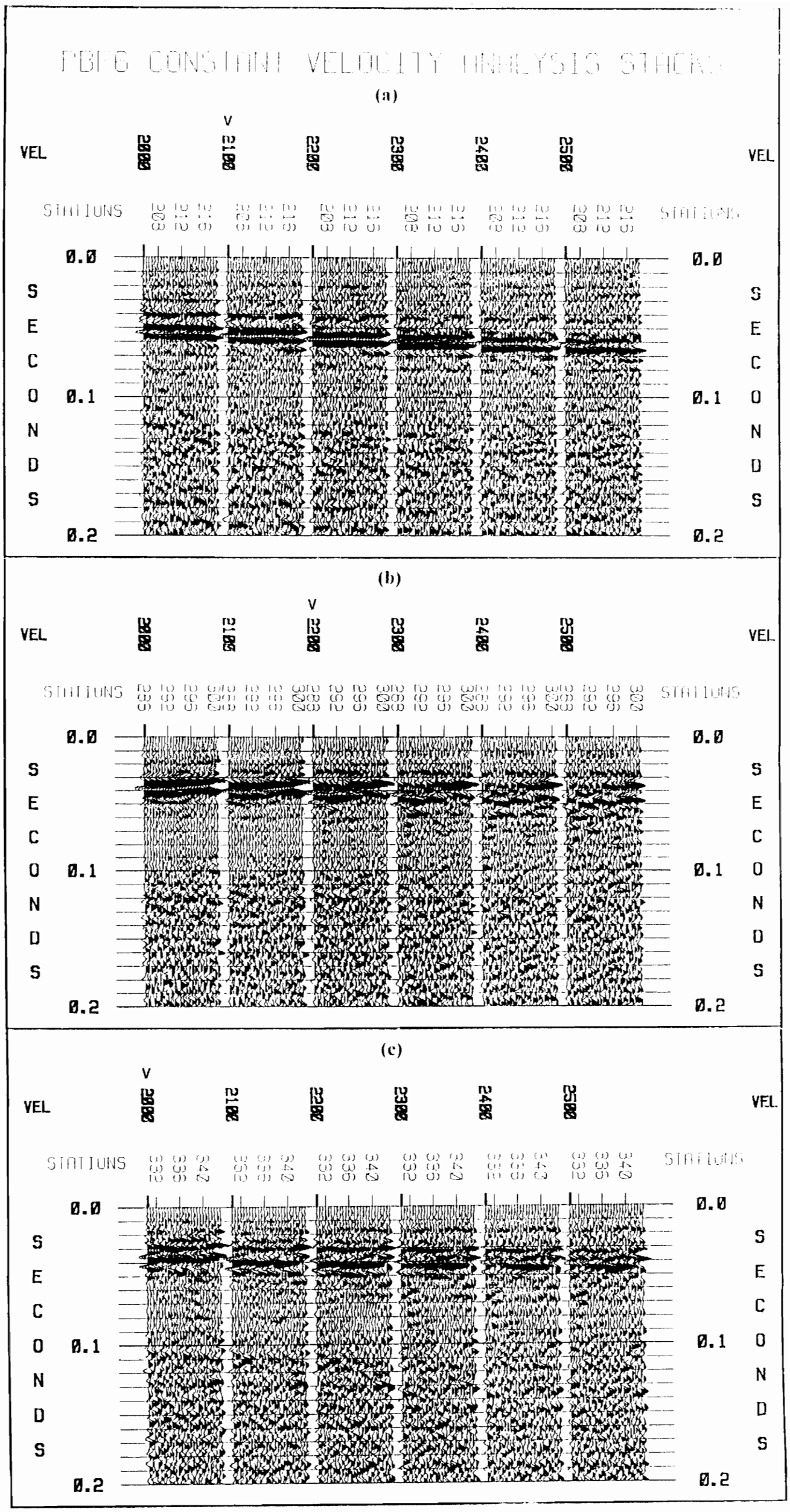

Figure 14. PBF line 6 constant velocity analysis panels for refractor B: Determination of refraction velocities at different station groups. Determining stacking velocities for the refractor in the refraction stack at different station groups. Examples of some of the panels used are shown for (a) stations 205-218, (b) stations 287-300 and (c) stations 330-343. V marks the velocity chosen for the refraction stack from that station group.

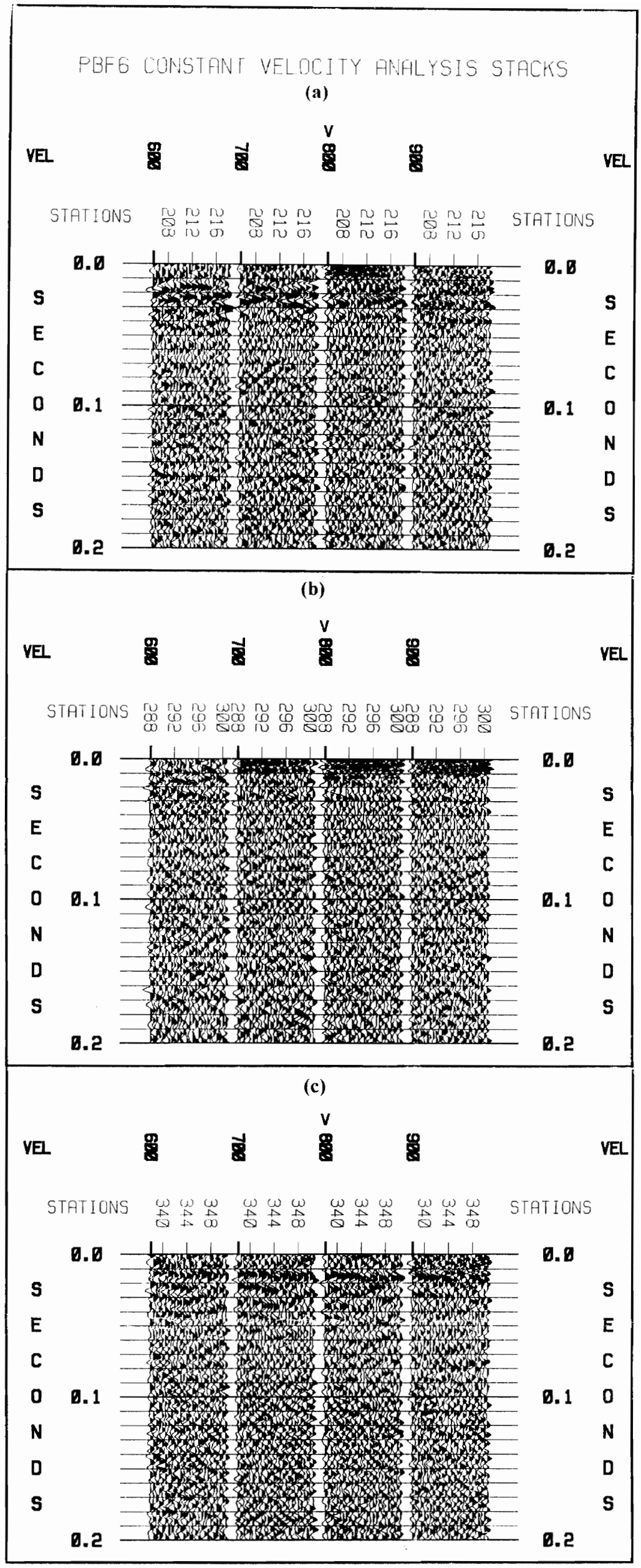

Figure 15. PBF line 6 constant velocity analysis panels: Determination of first layer velocity for depth calculation. The panels used are shown from (a) stations 205-218, (b) stations 288-300 and (c) stations 338-350. V marks the velocity chosen from that station group. A velocity of 800 m/s was used for the calculation.

refractor (B) are 28.8 m (station 200), 29.2 m (station 220), 24.0 m (station 270), 18.8 m (station 280) and 15.3 m (station 340). Fault displacements are about 5.0 m beneath station 275 in the second refractor (B) and about 4.0 m beneath station 265 in the first refractor (A).

In this area, Sen (1991) interprets the fault closer to station 250 and an antithetic fault near station 300 of PBF line 6. He also interprets a variation in thickness between stations 200 - 270, which gives a channel geometry, In Figure 16b, Çoruh and Costain (1994) interprets a deformation between stations 240 - 260. There is no clear deformation in the refraction stack (Figure 16a) in this area except possibly beneath station 250 in the second refractor (B). There might be disturbance in the reflector between stations 260 - 280 (Figure 16b) which would extend upward to correspond to the offsets in the refractors in the refraction stack (Figure 16a). In Figure 16c, the reflection stack of Domoracki (1995) shows possible offsets beneath the same stations. The reflectors dip down toward the northwest between stations 200 - 270. This dipping occurs in the other stacks of Figure 16. The Pen Branch Fault is interpreted to penetrate up beneath station 265 and/or 275, where there is a reverse sense of motion in the refraction stack (Figure 16a).

PBF line 13

The PBF line 13 trends from southwest to northeast for about 0.7 km (Figure 4). The refraction stack with 94 m datum and a velocity range of 1550 - 1750 m/s is shown in Figure 17. Examples of the constant velocity analysis panels and the final stacking velocities (indicated by V) are shown in Figure 18. The dominant feature is between stations 130 - 190 and this might be a stream channel (Figure 17). There are offsets beneath between stations 120 - 140. Using a velocity of 800 m/s (based on the constant velocity panels in Figure 19), the depths to the refractor from the surface are 7.0 m (station 120), 4.0 m (station 125), 8.0 m (station 130), 12.0 m (station 140), 12.0 m (station 160), 7.2 m (180) and 5.0 m (station 200). Fault displacement is about 4 m beneath station 130.

Berkman (1991) interprets the Pen Branch Fault near station 165 (shotpoint 130) and interpreted stream channels at greater depths along the line. There appears to be no offset or deformation near station 165 at this level in the refraction stack (Figure 20a) Çoruh and Costain (1994) interpret an offset beneath stations 120-130 from the reflection stack of this line (Figure

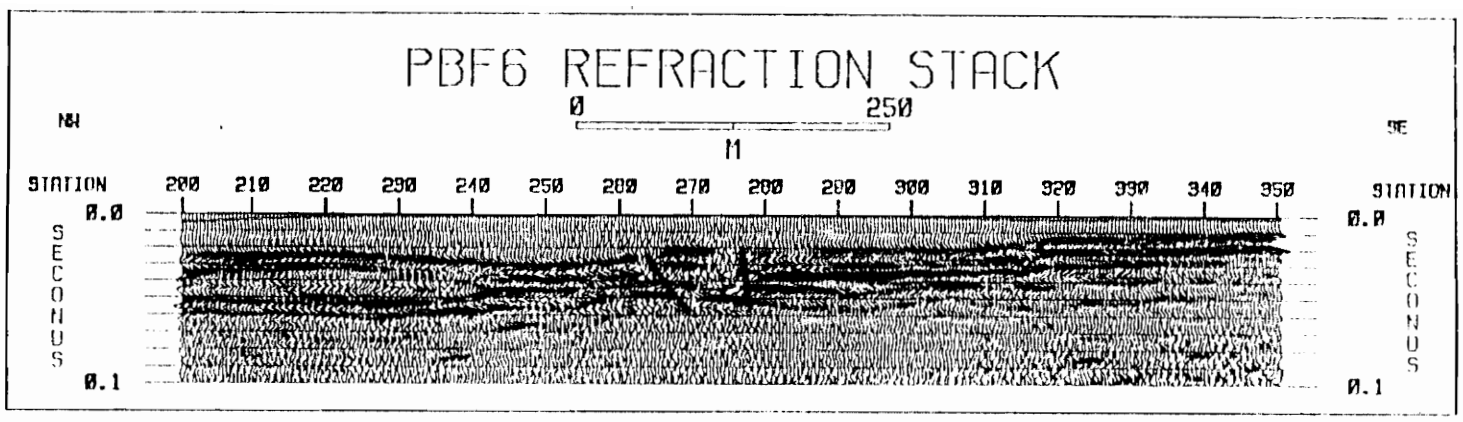

(a)

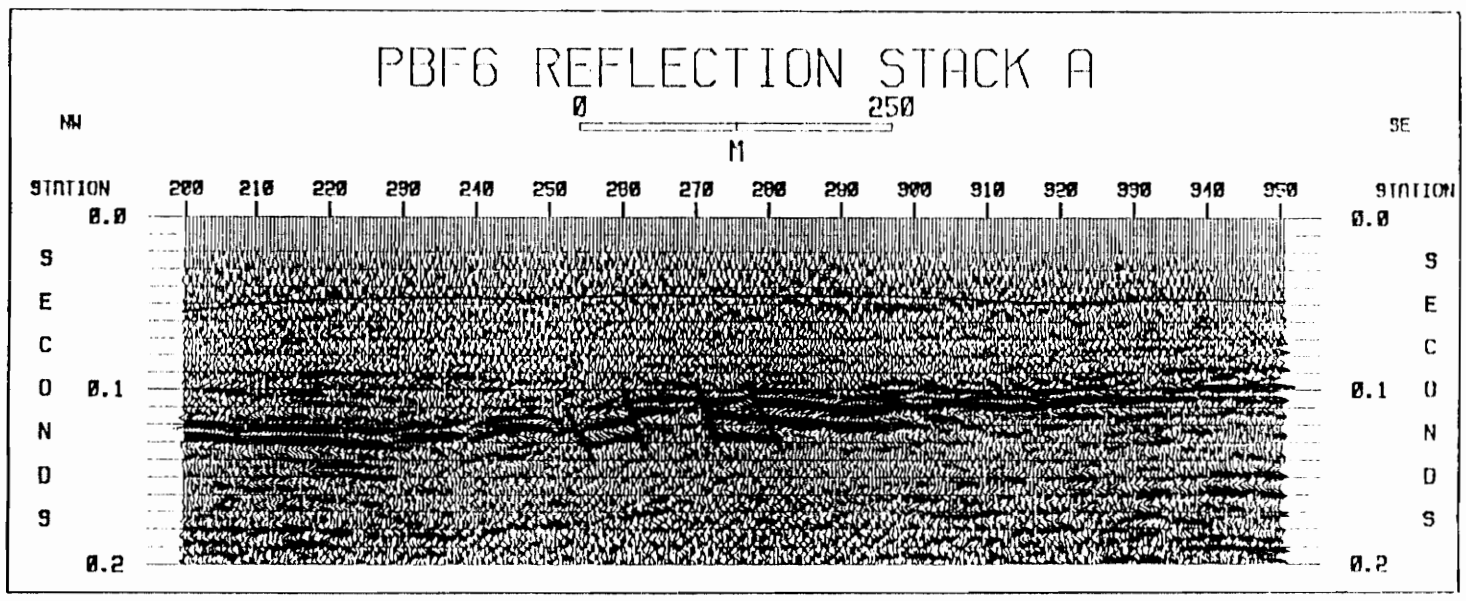

(b)

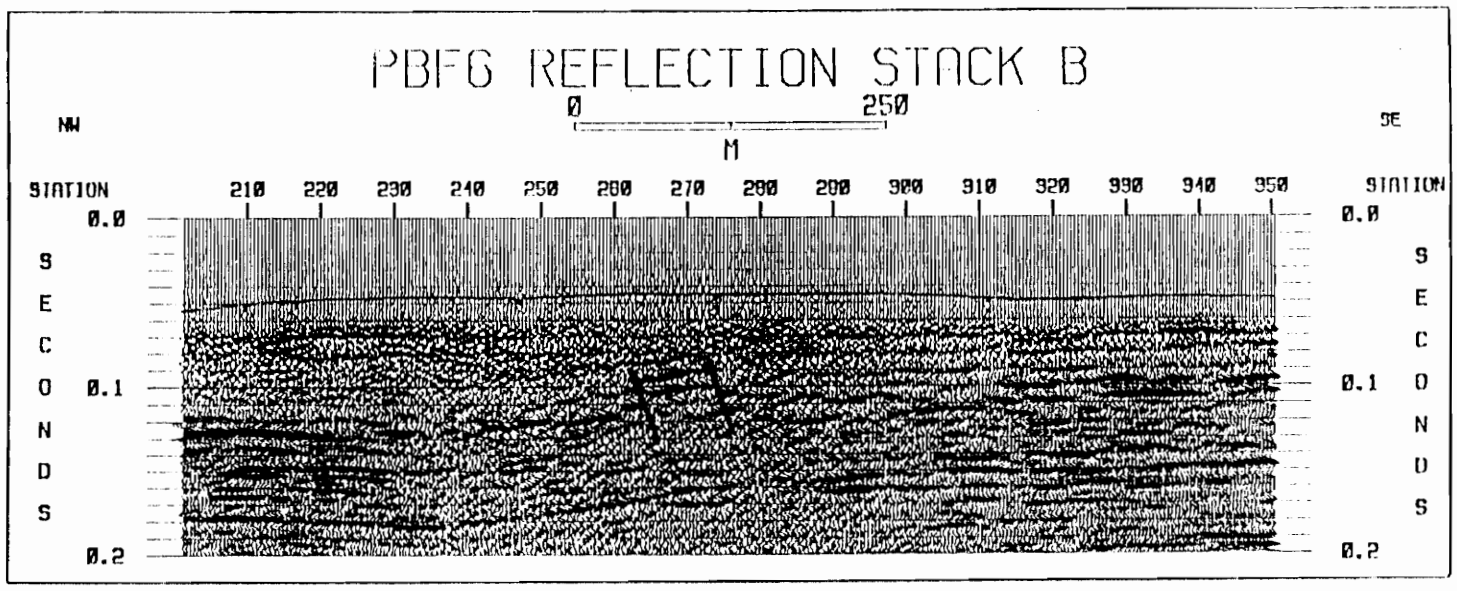

(c)

Figure 16. PBF line 6 refraction and reflection stacks: Comparison to determine any corresponding offsets and features at shallow depths in the refraction stack (94 m datum) shown in (a) and deeper events in the reflection stacks (80 m datum and 50 ms bulk shift) of Couch and Costain (1994) shown in (b) and of Domoracki (1995) shown in (c).

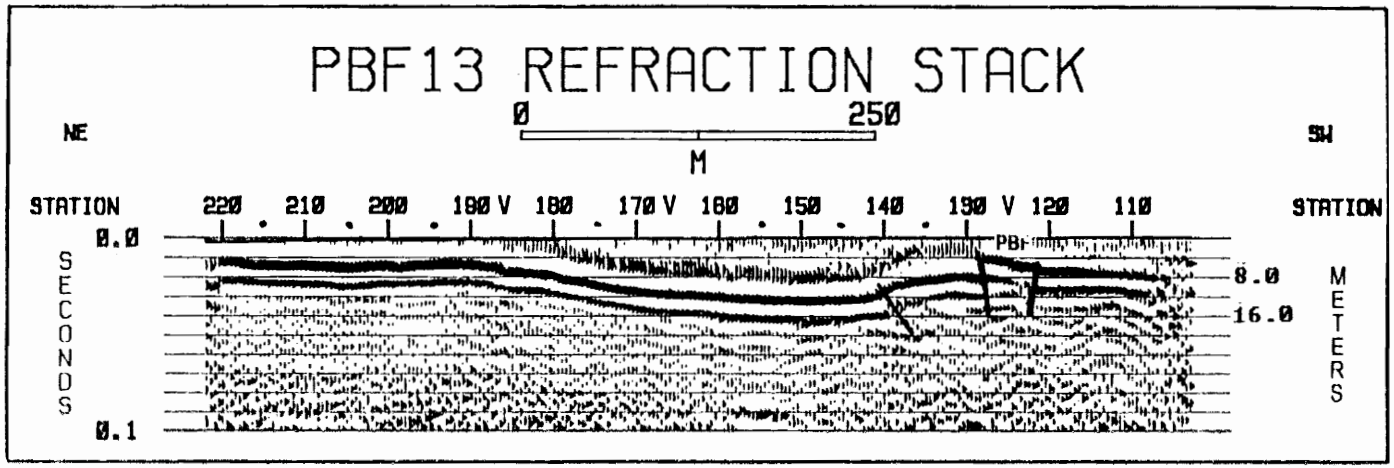

Figure 17. PBF line 13 refraction stack: The refraction stack was created with a 94 m datum and a velocity range of 1550-1750 m/s. V marks the location of stations used in the examples of the velocity analysis panels for determining stacking velocities shown in Figure 18. A point (•) marks the location of the other stations not included in the examples of the velocity analysis panels. Possible offsets are shown in the Pen Branch Fault zone. PBF = Pen Branch Fault.

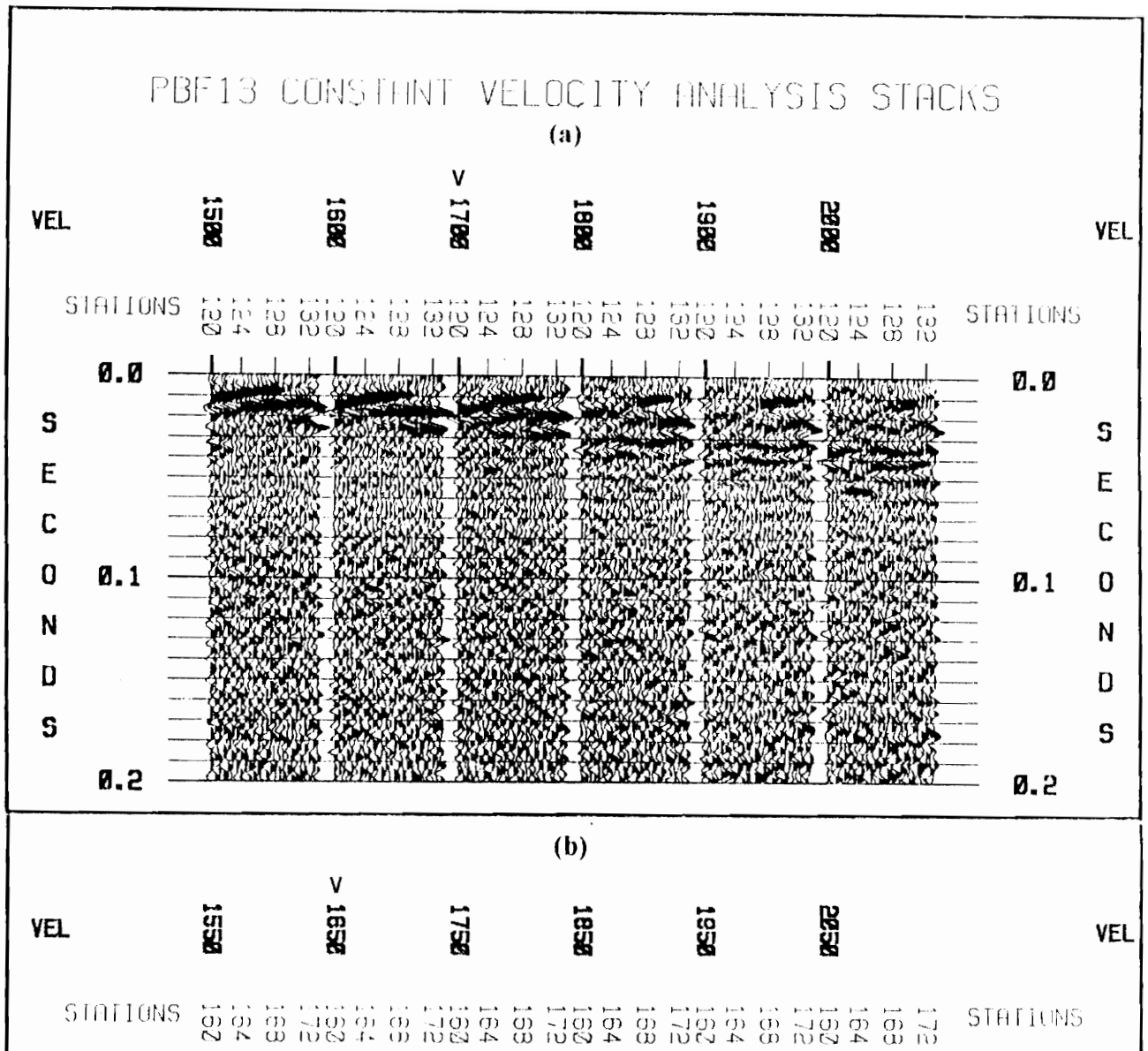

Figure 18. PBF line 13 constant velocity analysis panels: Determination of refraction velocities at different station groups. Examples of some of the panels used are shown for (a) stations 120-132, (b) stations 160-172 and (c) stations 183-195. V marks the velocity chosen for the refraction stack from that station group.

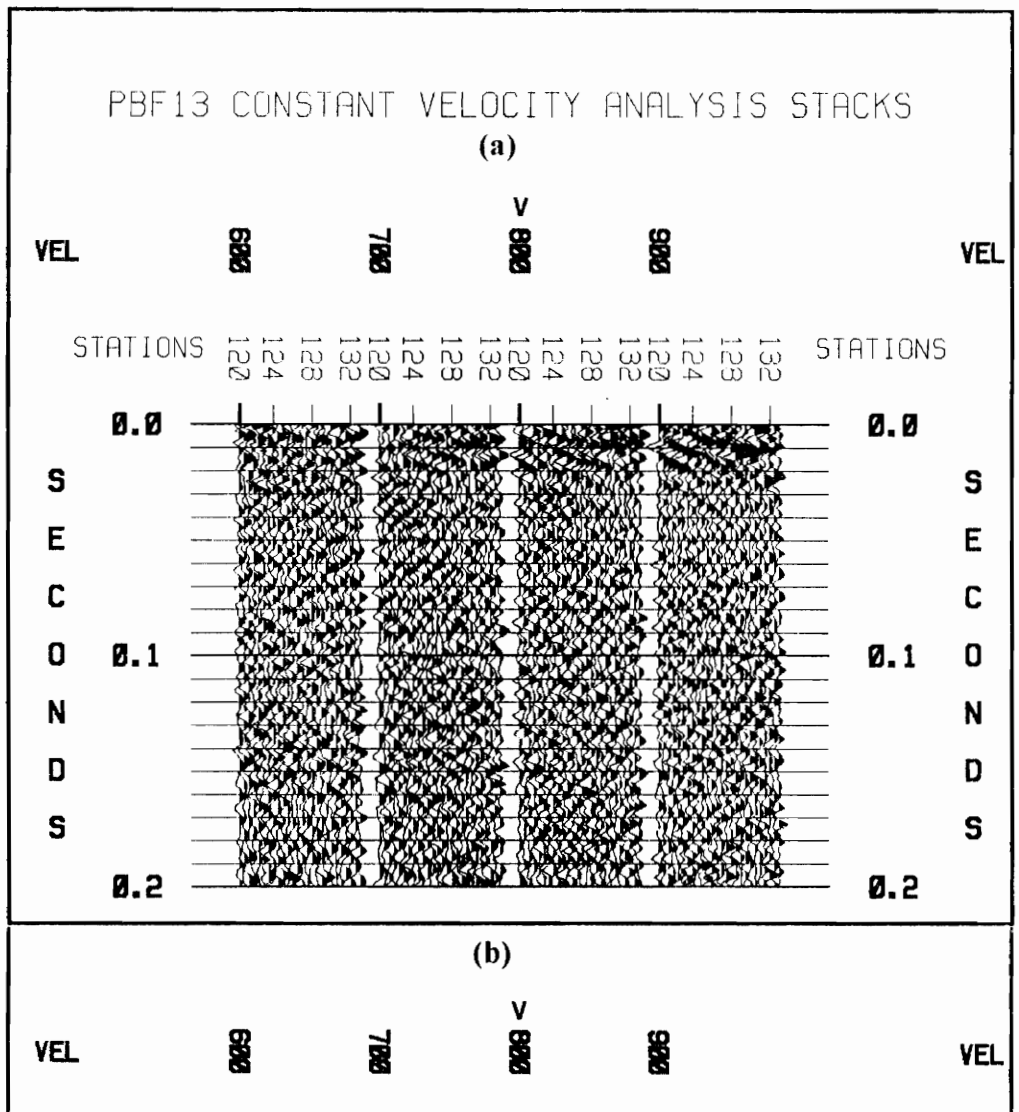

Figure 19. PBF line 13 constant velocity analysis panels: Determination of first layer velocity for depth calculation. The panels used are shown from (a) stations 120-132, (b) stations 145-158 and (c) stations 195-208. V marks the velocity chosen from that station group. A velocity of 800 m/s was used for the calculation.

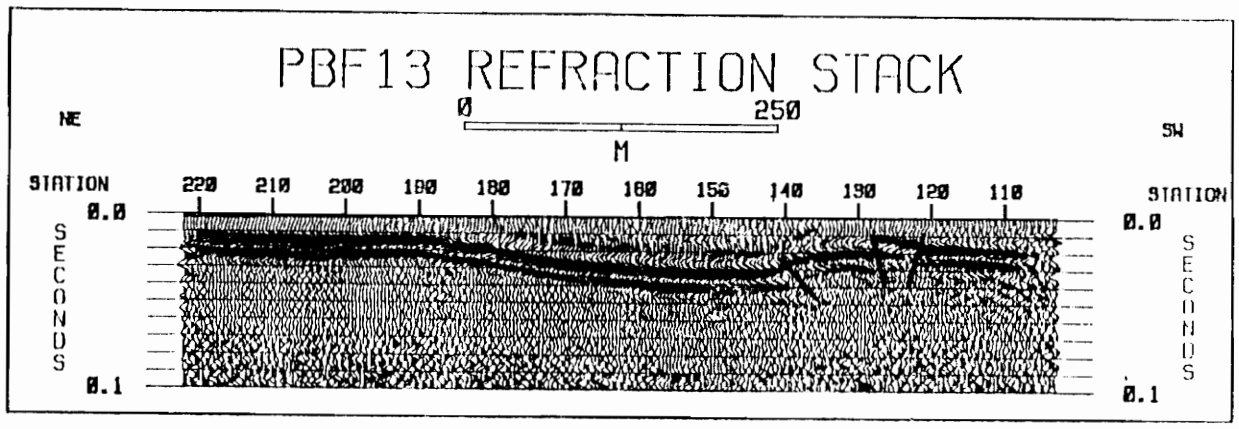

(a)

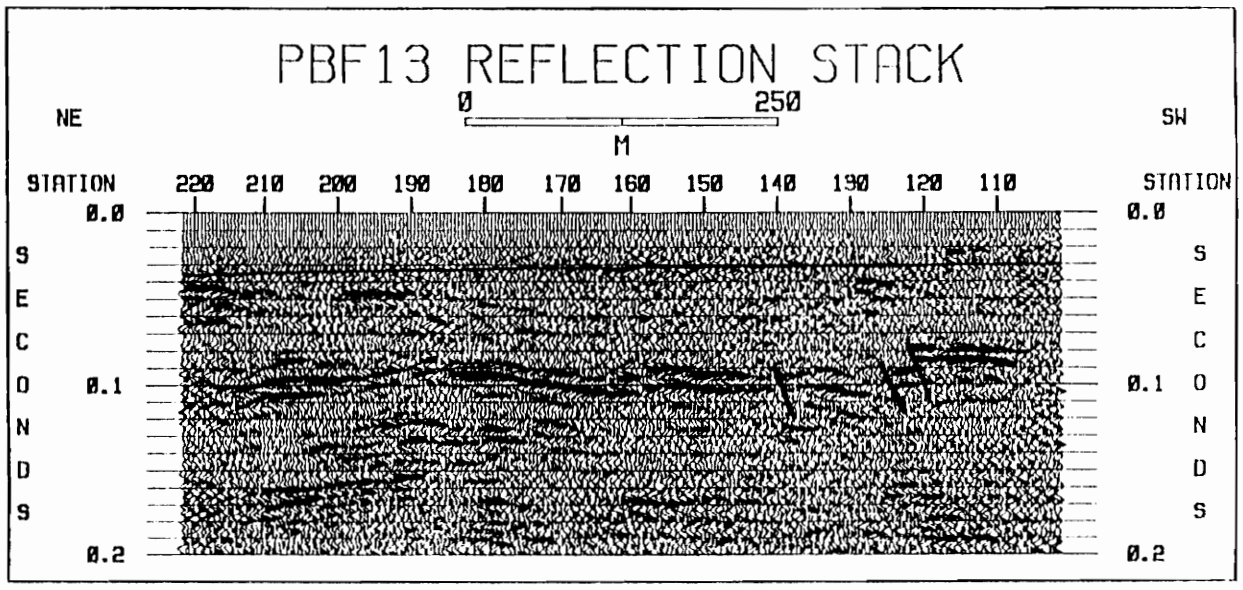

(b)

Figure 20. PBF line 13 refraction and reflection stacks: Comparison to determine any corresponding offsets and features at shallow depths in the refraction stack (94 m datum) shown in (a) and deeper events in the reflection stack (80 m datum and 50 ms bulk shift) of Couch and Costain (1994) shown in (b).

20b) and possibly an offset or just deformation beneath station 140. They interpreted the reflector between 90 to 100 ms is correlative with the base of the Santee and top of the Congaree near the so-called "green clay". The Pen Branch Fault is interpreted to correspond to the offset showing reverse motion beneath station 128 in the refraction stack (Figure 20a).

PBF line 12

The PBF line 12 along SRS line 3 extends from southeast to northwest then turns generally to the north (Figure 4). The portion of PBF line 12 reprocessed is from stations 101 - 360, a length of about 1.6 km. A larger turn in the line occurs between stations 160 - 200 and a smaller one between stations 280 - 300. The refraction stack with 105 m datum and velocity range of 1650 - 1750 m/s is shown in Figure 21. Examples of the constant velocity analysis panels and the final stacking velocities (indicated by V) are shown in Figure 22. The data quality is generally good, but there is a low fold beneath station 305 causing poor resolution. Also the data may be affected around the turns of the line (stations 160 - 200 and 280 - 300). Possible fault offsets are near stations 195 and 205 (Figure 21). These offsets have a slight upthrown side on the southern side. Using an average velocity of 850 m/s (based on constant velocity panels in Figure 23), the depths to the refractor from the surface are 15.3 m (station 110), 10.3 m (station 170), 11.0 m (station 205), 11.7 m (stations 210), 11.0 m (station 220), and 10.6 m (station 260), 11.7 m (station 270), 11.0 m (station 280) and 7.6 m (station 340). Average displacements are about 1.3 m (station 195) and 1.0 m (station 205).

Other interpretations of PBF line 12 include Berkman (1991) who interprets the Pen Branch Fault to be near station 165 (shotpoint 130) and Çoruh and Costain (1994) interprets the fault near stations 210-220 (Figure 24b). Because PBF line 12 overlies SRS line 3, a portion of the SRS line 3 from Domoracki (1995) is included in Figure 25. The part of PBF line 12 reprocessed corresponds to about stations 936 to 1063 of SRS line 3. An offset is interpreted for the Pen Branch Fault from the top of basement at 0.4 s, which is about 0.33 s (about 300 m) below the surface, and upward beneath station 950 to about 0.18 s (about 130 m) below the surface. Station 950 of SRS line 3 corresponds to about station 127 in PBF line 12. There appears to be no strong evidence of a corresponding offset or even deformation in the refraction stack in this area (Figure 24a). Possibly a branch of the Pen Branch Fault in SRS line 3 extends up to

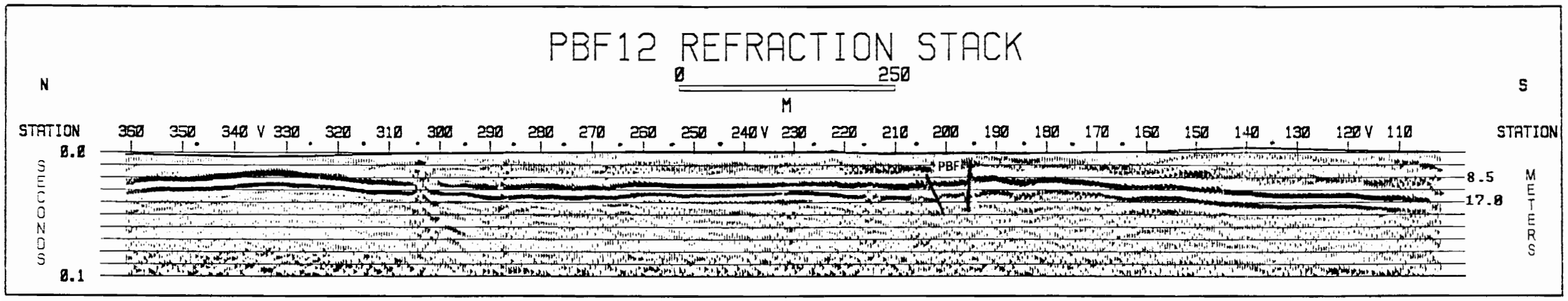

Figure 21. PBF line 12 refraction stack: The refraction stack was created with a 105 m datum and a velocity range of 1650-1750 m/s. V marks the location of stations used in the examples of the velocity analysis panels for determining stacking velocities shown in Figure 22. A point (•) marks the location of the other stations not included in the examples of the velocity analysis panels. Possible offsets are shown in the Pen Branch Fault zone. PBF = Pen Branch Fault.

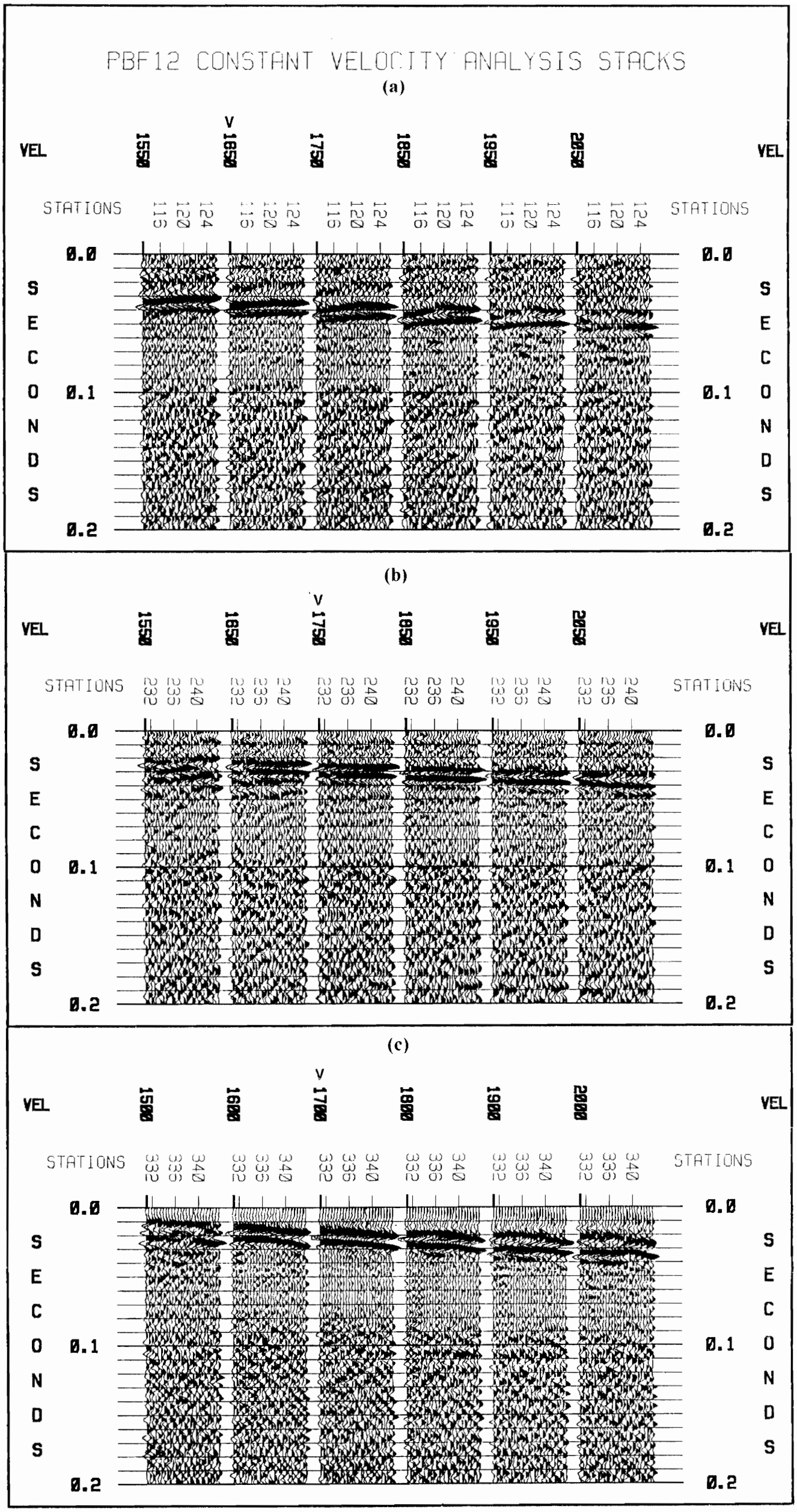

Figure 22. PBF line 12 constant velocity analysis panels: Determination of refraction velocities at different station groups. Examples of some of the panels used are shown for (a) stations 113-125, (b) stations 231-243 and (c) stations 331-343. V marks the velocity chosen for the refraction stack from that station group.

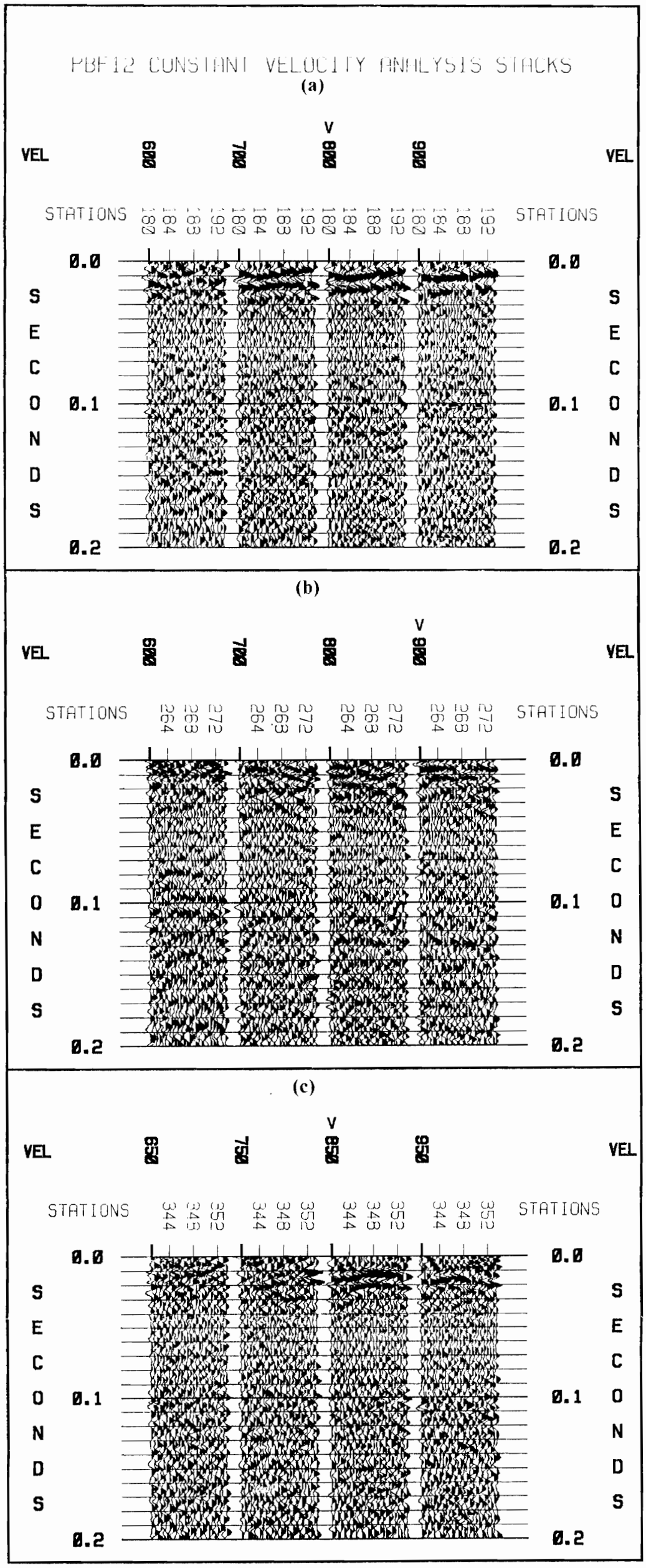

Figure 23. PBF line 12 constant velocity analysis panels: Determination of first layer velocity for depth calculation. The panels used are shown from (a) stations 180-192, (b) stations 261-273 and (c) stations 341-353. V marks the velocity chosen from that station group. An average of 850 m/s was used for the calculation.

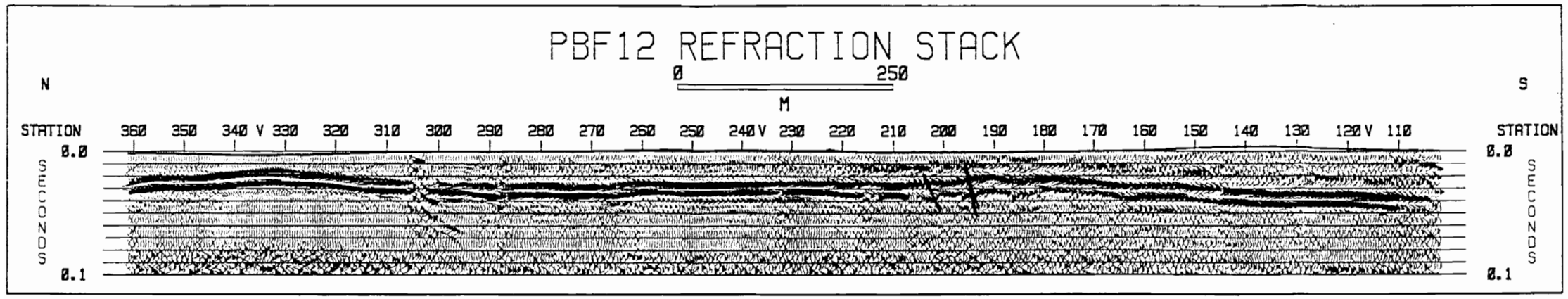

(a)

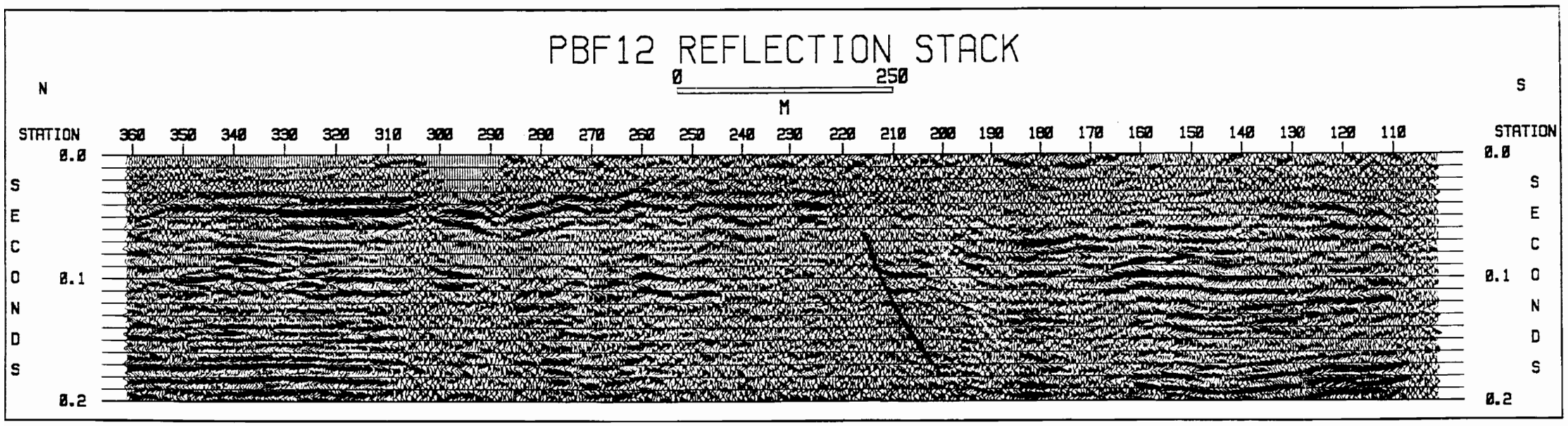

(b)

Figure 24. PBF line 12 refraction and reflection stacks: Comparison to determine any corresponding offsets and features at shallow depths in the refraction stack (105 m datum) shown in (a) and deeper events in the reflection stack (80 m datum and no bulk shift) of Çoruh and Costain (1994) shown in (b).

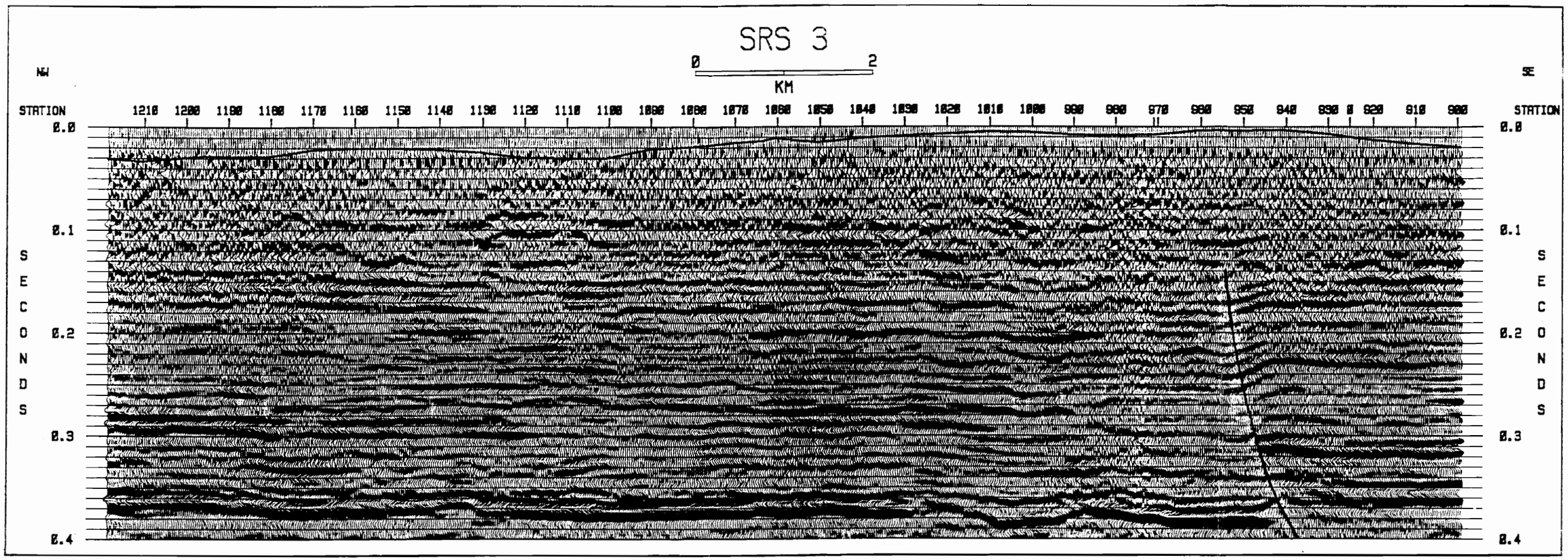

Figure 25. SRP line 3 reflection stack: PBF line 12 overlays SRP line 3. Portion of the reflection stack from Domoracki (1995) is shown. The offset beneath between stations 940 and 950 may be the Pen Branch Fault which corresponds around the beginning of PBF line 12.

where an offset occurs in the refraction stack.. Sen (1991) has processed the SRS line 3 and interprets the fault to be near station 985 with an antithetic fault at station 945. Station 985 of SRS line 3 is along station 202 on PBF line 12. This may correspond to the possible offset beneath stations 190 - 210 in the refraction stack (Figure 24a) with a reverse fault displacement at this depth.

PBF line 11

The reprocessed portion of the northwest to southeast trending PBF line 11 is from stations 101 to 290 with about a 1.1 km length (Figure 4). The refraction stack with a datum of 105 m and a velocity range of 1650 - 1750 m/s is shown in Figure 26. Examples of the constant velocity panels and the final stacking velocities (indicated by V) are shown in Figure 27. The data quality is poor to good. There is a possible offset near stations 205 - 210 (Figure 26), where a reverse fault is interpreted. PBF line 11 shows the upthrown side on the southern side of the interpreted fault as did the PBF lines 6, 12, and 13. Other offsets might also be interpreted near stations 260 - 270. There may be a stream channel between stations 160 - 190 but the resolution is poor for the refractor in this area. Offsets on the southern side of a channel-like feature are similar to features in PBF lines 6 and 13. The sediments seem to dip in the direction of the regional dip of the ACP sediments. Using a velocity of 800 m/s (from constant velocity analysis panels shown in Figure 28), the depths to the refractor are 5.6 m (station 120), 8.5 m (station 140), 11.4 m (station 180), 12.7 m (station 220) and 15.7 m (station 240). The fault displacement near stations 205 - 210 is about 1.3 m. Other interpretations of these data (Berkman, 1991; Çoruh and Costain, 1994) do not suggest evidence of faulting, though Berkman does point out an antiformal structure in deeper depths. In PBF line 18, Çoruh and Costain (1994) interpret the Pen Branch Fault below 0.25 s (two-way traveltime) between stations 203 and 243. Domoracki (1995) interprets the fault between stations 240 - 260, about 0.14 s (about 110 m) below the surface, where the yellow horizon is. The Pen Branch Fault is probably associated with the possible offset with reverse motion between stations 205 - 210 in the refraction stack in this study (Figure 26).

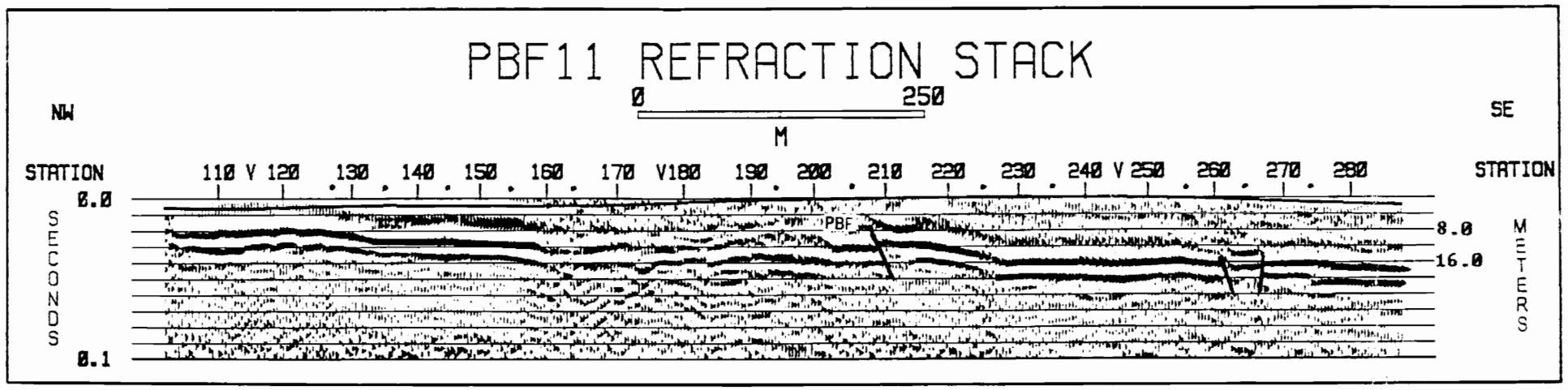

Figure 26. PBF line 11 refraction stack: The refraction stack was created with a 105 m datum and a velocity range of 1650-1750 m/s. V marks the location of stations used in the examples of the velocity analysis panels for determining stacking velocities shown in Figure 27. A point (•) marks the location of the other stations not included in the examples of the velocity analysis panels. Possible offsets are shown in the Pen Branch Fault zone. PBF = Pen Branch Fault.

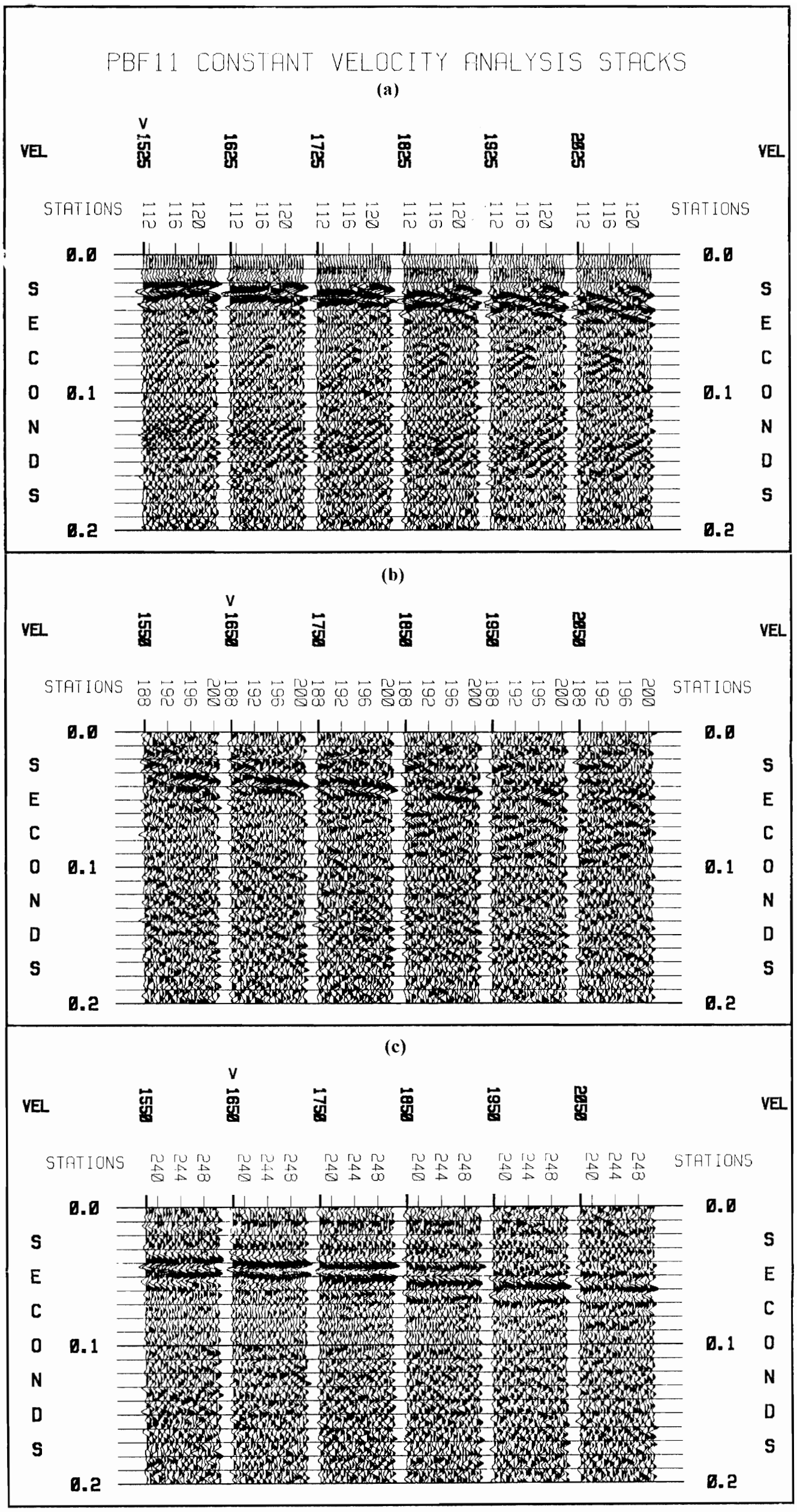

Figure 27. PBF line 11 constant velocity analysis panels: Determination of refraction velocities at different station groups. Examples of some of the panels used are shown for (a) stations 110-123, (b) stations 188-200 and (c) stations 238-250. V marks the velocity chosen for the refraction stack from that station group.

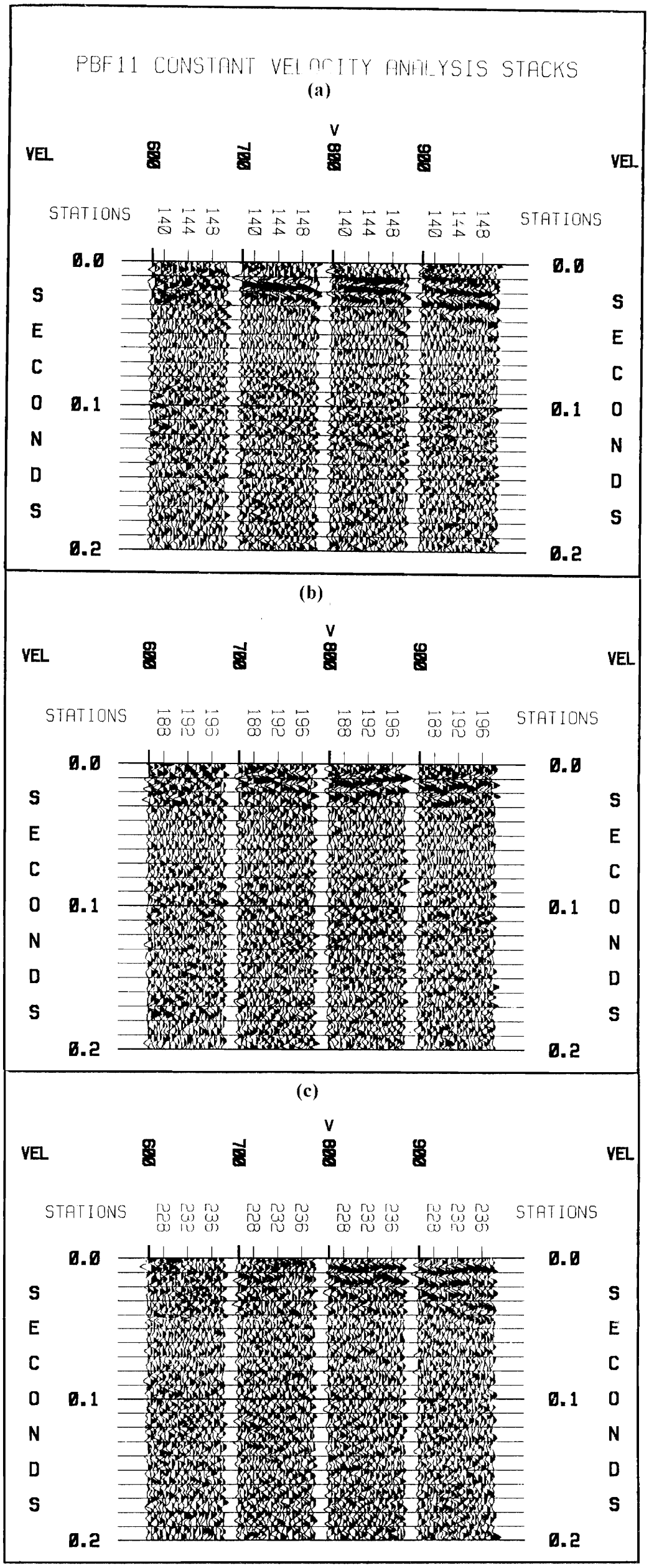

Figure 28. PBF line 11 constant velocity analysis panels: Determination of first layer velocity for depth calculation. The panels used are shown from (a) stations 138-150, (b) stations 188-200 and (c) stations 225-238. V marks the velocity chosen from that station group. A velocity of 800 m/s was used for the calculation.

PBF line 17

PBF line 17 runs southwest to northeast for about 1.6 km. The refraction stack with a datum of 77 m and velocity range of 1750-1800 m/s is shown in Figure 29. Examples of the constant velocity analysis panels and the final stacking velocities (indicated by V) are shown in Figure 30. The data quality in the stack section was fair to good and resulted in an undulating event with some apparent discontinuities. These possible discontinuities or offsets are near stations 180 and 215 (Figure 29). Offsets at stations 180 and 215 are interpreted as reverse faults, the southwest sides upthrown. Most likely there is deformation between station 260 - 280 at this level. Using a velocity of 800 m/s that was used for most of the other lines, the depths to the refractors are 16.8 m (station 170), 16.4 m (station 260), and 17.6 m (station 320). Displacements along this event vary from about 3.4 m (station 180) to 1.1 m (station 215).

Interpretations of others are also used to help decipher the location of the Pen Branch Fault on this line. Berkman (1991) interprets the Pen Branch Fault near station 222 but it penetrated only up to the base of the Cape Fear Formation. He also points out that there are possible stream channels or meanders causing irregular dipping events. This may also be true in shallower events in the refraction stack (Figure 31a). The dipping events forming structures between stations 215 - 235 and 245 - 265 in the refraction stack (Figure 31a) might be stream channels. Çoruh and Costain (1994) interpret an offset beneath station 255 of a reflection stack (Figure 31b) at about 85 ms from the surface. A relative high in the northeast beneath station 265 in the reflection stack is similar to the one in the refraction stack between stations 260 and 280 (Figure 31a). There also seems to be deformation, possibly an offset, beneath stations 200 - 210 in the reflection stack (Figure 31b) which might correspond to the offset between stations 210 - 215 in the refraction stack (Figure 31a). Berkman's (1991) interpretation of the offset may also correspond to the offset in the refraction stack at station 215. The offset interpreted in Çoruh and Costain (1994) will correspond to about station 260 in the refraction stack. However, in the refraction stack section (Figure 31a), it is difficult to interpret a fault at this level but deformation may be possible. Based on other interpretations of the lines that surround PBF line 17, the Pen Branch Fault should be located through the area between stations 200 - 300 in PBF line 17. SRS lines 1 and 23 are in the vicinity of PBF line 17. Sen (1991) interprets the Pen

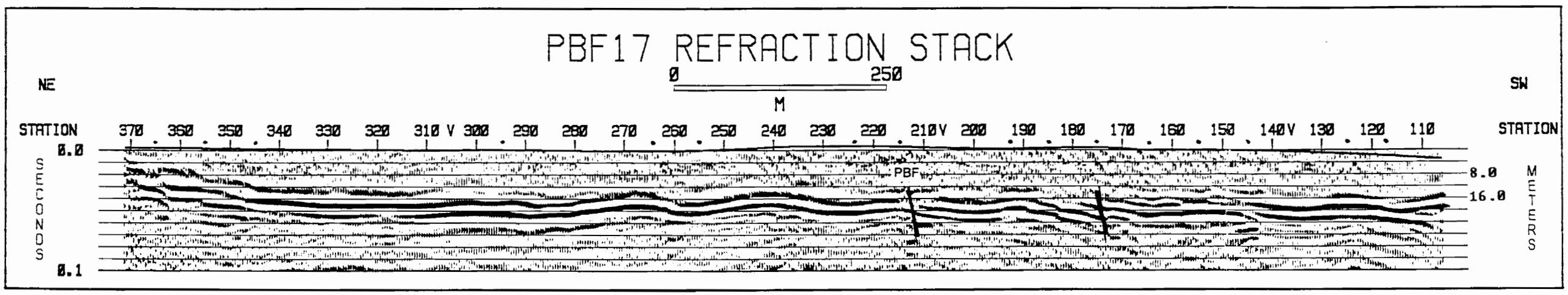

Figure 29. PBF line 17 refraction stack: The refraction stack was created with a 77 m datum and a velocity range of 1750-1800 m/s. V marks the location of stations used in the examples of the velocity analysis panels for determining stacking velocities shown in Figure 30. A point (•) marks the location of the other stations not included in the examples of the velocity analysis panels. Possible offsets are shown in the Pen Branch Fault zone. PBF = Pen Branch Fault.

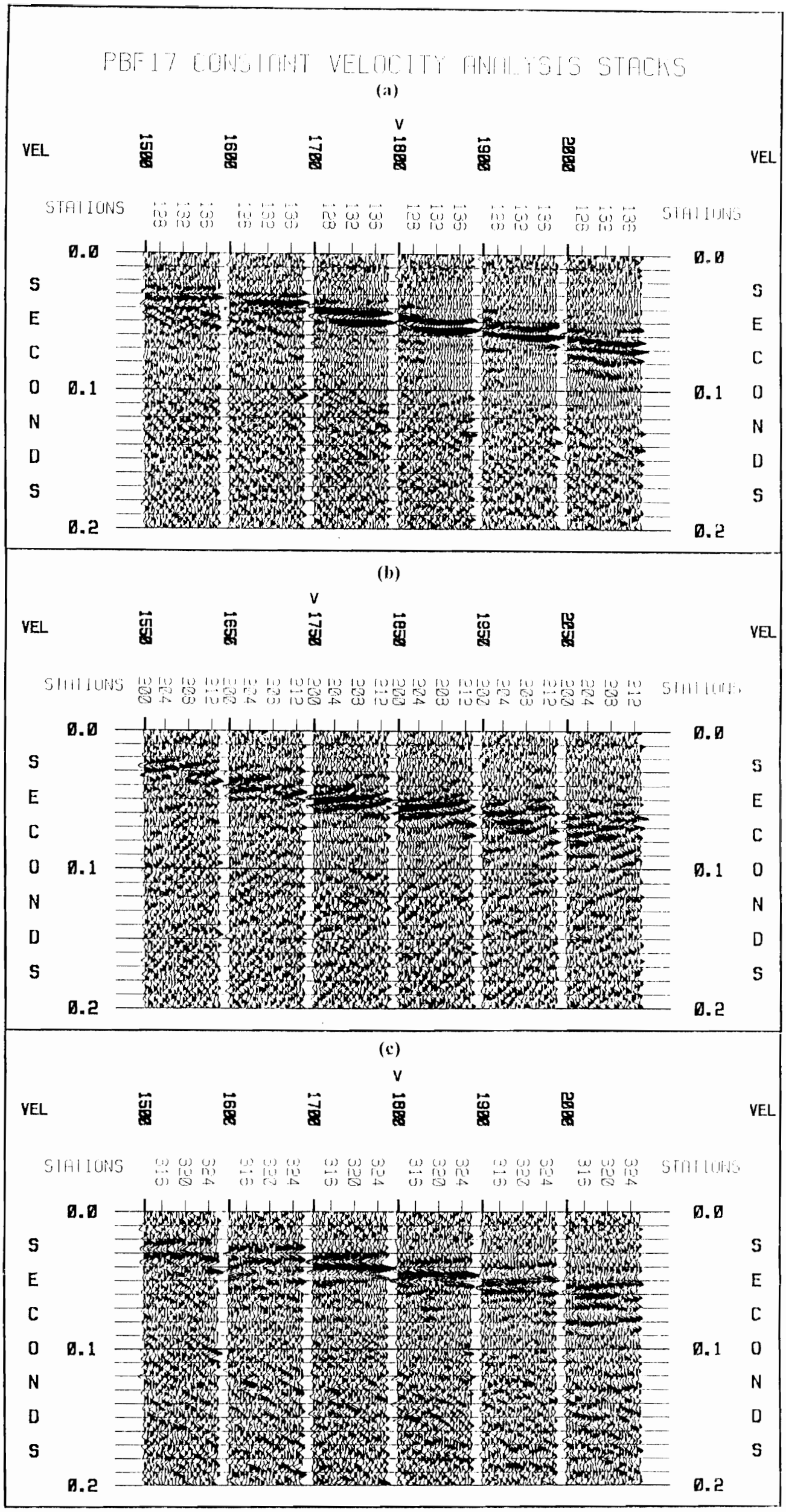

Figure 30. PBF line 17 constant velocity analysis panels: Determination of refraction velocities at different station groups. Examples of some of the panels used are shown for (a) stations 125-138, (b) stations 200-213 and (c) stations 313-326. V marks the velocity chosen for the refraction stack from that station group.

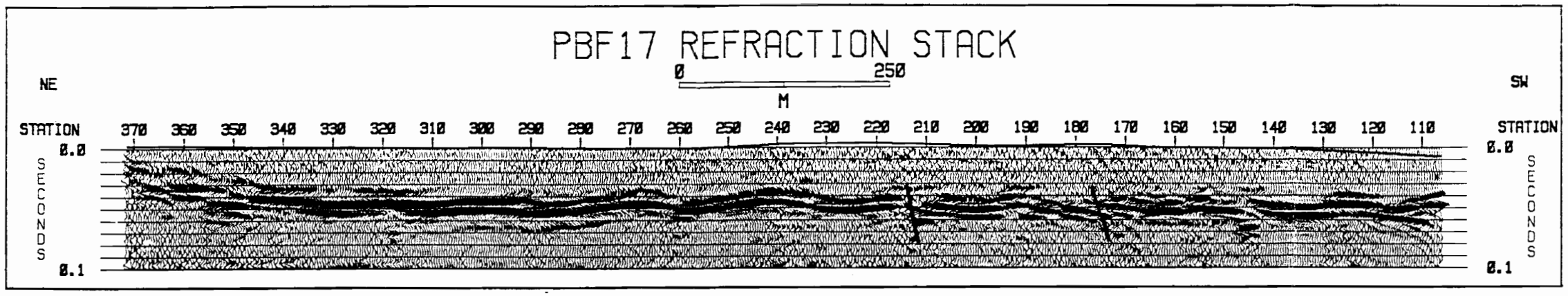

(a)

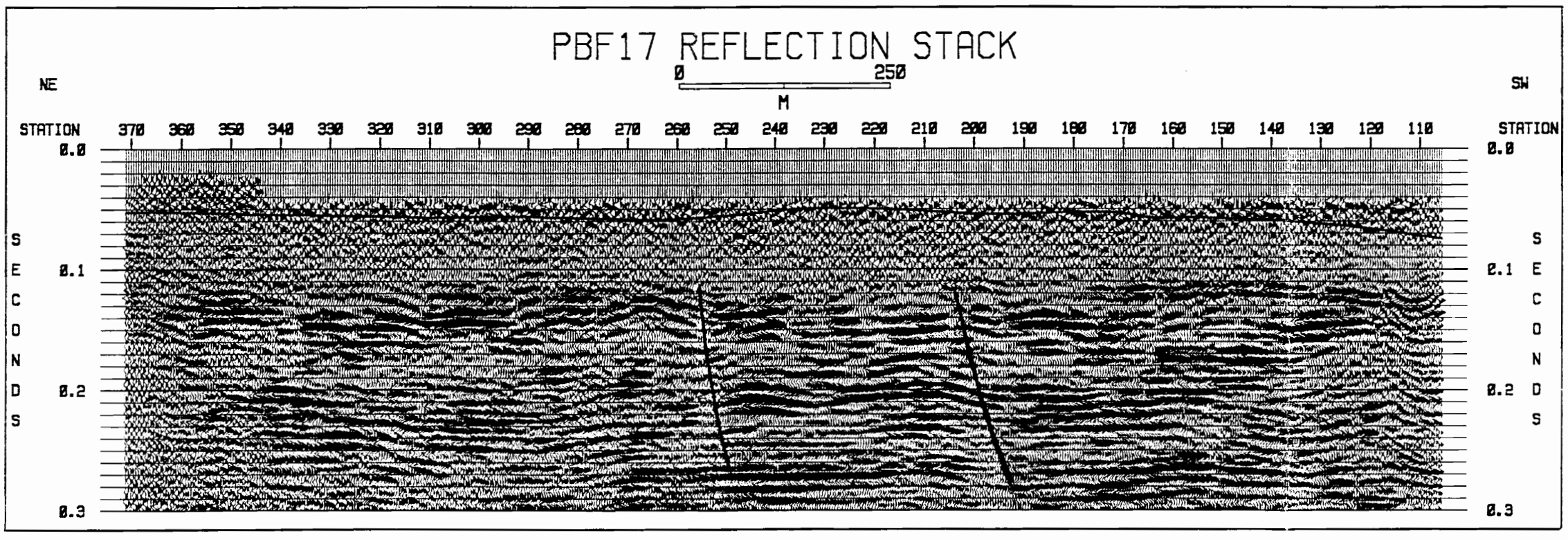

(b)

Figure 31. PBF line 17 refraction and reflection stacks: Comparison to determine any corresponding offsets and features at shallow depths in the refraction stack (77 m datum) shown in (a) and deeper events in the reflection stack (80 m datum and 50 ms bulk shift) of Çoruh and Costain (1994) shown in (b).

Branch Fault in SRS line 1 to be between stations 900 - 930 about 0.17 s (two-way traveltime) (about 123 m) below the surface and to be associated with small antithetic normal faults. Domoracki (1995) interprets the fault in the same line as being between stations 900 - 950, about station 925 at about 0.16 s (about 116 m) below the surface. For SRS line 23, Sen (1991) interpreted the fault near station 125 about 0.16 s (about 116 m) below the surface and an antithetic fault near station 90 around 0.14 s (about 105 m) below the surface. Domoracki interprets offsets between stations 190 - 200 and 95 - 100 on SRS line 23 . A possible location of the Pen Branch Fault could be about station 215 in the refraction stack (Figure 31a).

Borehole Correlations

An attempt was made to correlate the refraction stack sections with borehole log data from the PBF boreholes (Figure 4) also used by Berkman (1991). The boreholes were not in close proximity for the lines processed for this study; however correlations between the refraction stack sections and logs are attempted for PBF lines 6, 11 and 12. Synthetic seismograms were generated from sonic and density logs (after editing, changing of units, adjusting datum and filling to the surface), using a zero-phase Ricker wavelet of 120 Hz. Log processing was done using CogniSeis' Digital Log Processing System (DLPS) software. Boreholes PBF-1 and PBF-2, PBF-3, and PBF-8 were correlated with PBF lines 6, 12 and 11, respectively. Only the first 100 ms of the refraction stack section was used for correlations with the synthetic traces. Available reference markers based on lithologic tops defined by Berkman (1991) and Fallow and Price (1992), were adjusted to datum used in the data processing for each line.

The correlations between boreholes PBF-1 and PBF-2 and PBF line 6 are shown in Figures 32 - 35. The reference markers are adjusted to a 80 m datum. On the northwest side of the interpreted fault in PBF line 6, borehole PBF-1 is correlated at CMP 862 (station 215.5). The Berkman (1991) based lithology markers associate the refractors to sediments above the Tan Clay, which is associated with the Twiggs Clay of the Dry Branch Formation (Figure 32). The Fallow and Price based lithology markers associate the refractor A closer to the Tobacco Road Sand and refractor B to the Irwinton (Dry Branch Formation) (Figure 33). On the southeast side of the fault, borehole PBF-2 is correlated at CMP 1222 (station 305.5). The Berkman (1991)

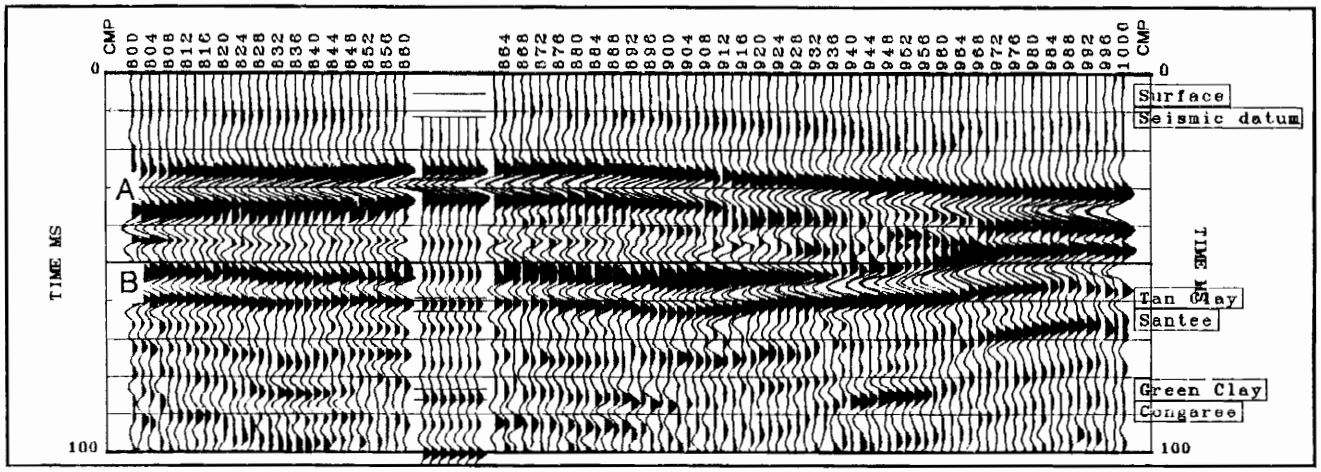

Figure 32. Synthetic seismogram from well PBF-1 correlated with PBF line 6: The correlation with PBF line 6 (stations 200 - 250) is at CMP 862 (station 215.5). The reference markers are corresponding to Berkman (1991) lithologies. A 80 m datum was used in processing both data sets.

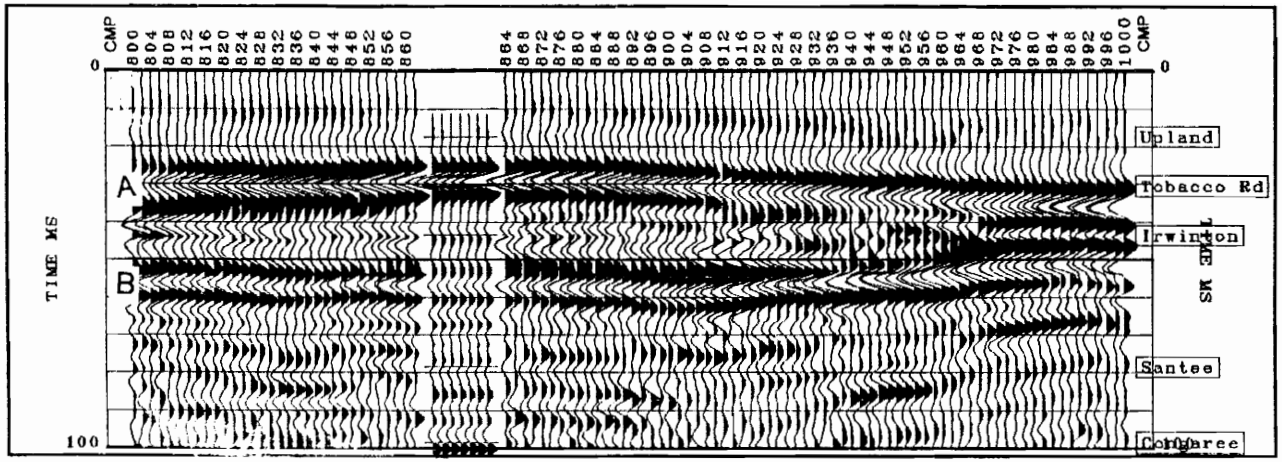

Figure 33. Synthetic seismogram from well PBF-1 correlated with PBF line 6: The correlation with PBF line 6 (stations 200 - 250) is at CMP 862 (station 215.5). The reference markers are corresponding to Fallow and Price (1992) lithologies. A 80 m datum was used in processing both data sets.

markers continue to associate the refractors above the Tan Clay (Figure 34). The Fallow and Price (1992) markers associate Irwinton closer to the refractor B (Figure 35). The correlation between borehole PBF-3 and PBF line 12 at CMP 957 (Station 239) is shown in Figures 36 and 37. The reference markers for this borehole are adjusted to a 105 m datum. The Berkman markers associate the refractor here to sediments above the Santee (Figure 36). The Fallow and Price markers associate the refractor with the younger Tobacco Road Sand (Figure 37). The correlation between borehole PBF-8 and PBF line 11 at CMP 866 (Station 216.5) is shown in Figures 38 and 39. The reference markers are also adjusted to a 105 m datum. The Berkman markers associate the refractor above the Tan Clay (Dry Branch Formation) (Figure 38). The Fallow and Price markers associate the same refractor above the Irwinton (Figure 39).

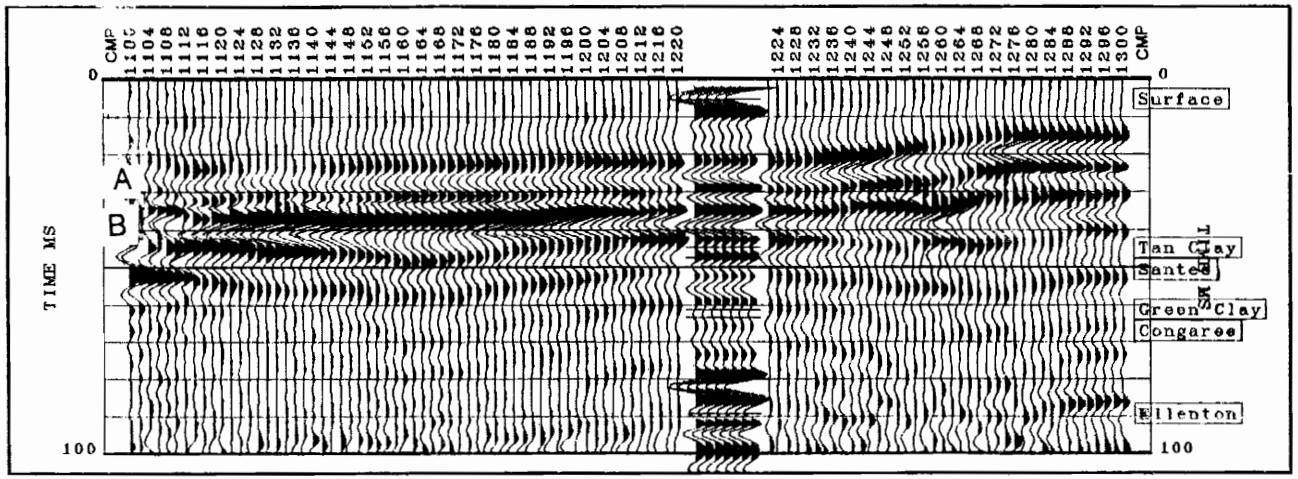

Figure 34. Synthetic seismogram from well PBF-2 correlated with PBF line 6: The correlation with PBF line 6 (stations 275 - 325) is at CMP 1222 (station 305.5). The reference markers are corresponding to Berkman (1991) lithologies. A 80 m datum was used in processing both data sets.

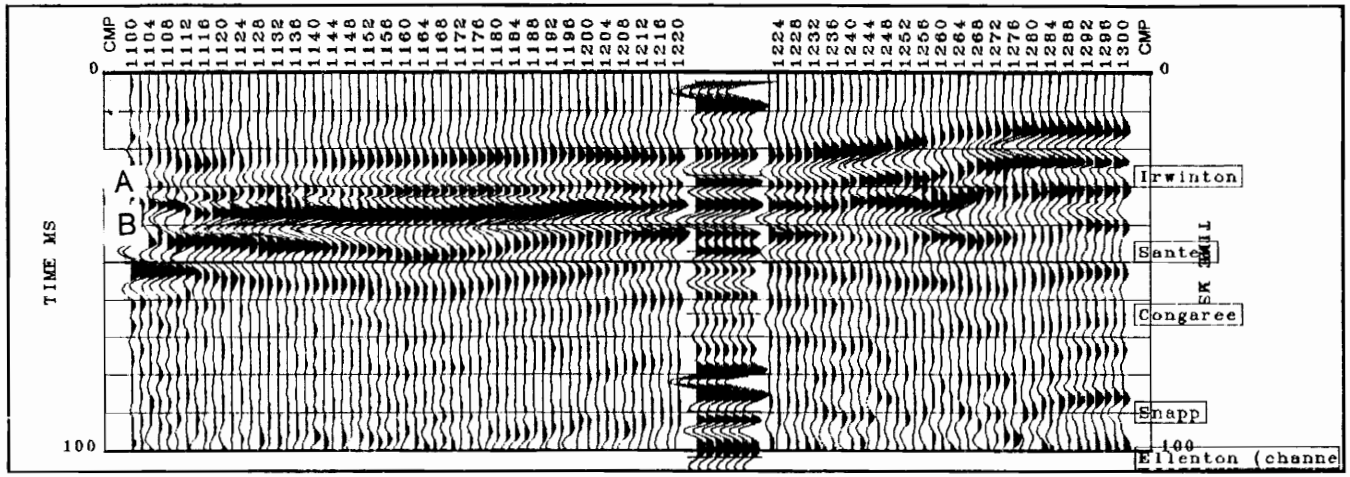

Figure 35. Synthetic seismogram from well PBF-2 correlated with PBF line 6: The correlation with PBF line 6 (stations 275 - 325) is at CMP 1222 (station 305.5). The reference markers are corresponding to Fallow and Price (1992) lithologies. A 80 m datum was used in processing both data sets.

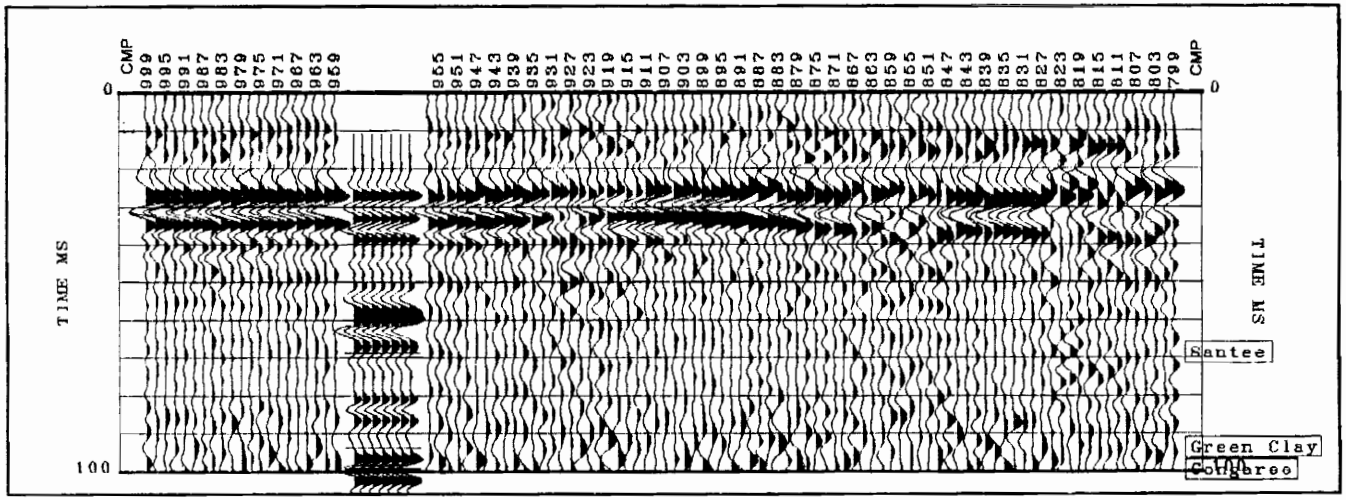

Figure 36. Synthetic seismogram from well PBF-3 correlated with PBF line 12: The correlation with PBF line 12 (stations 200 - 250) is at CMP 957 (station 239). The reference markers are corresponding to Berkman (1991) lithologies. A 105 m datum was used in processing both data sets.

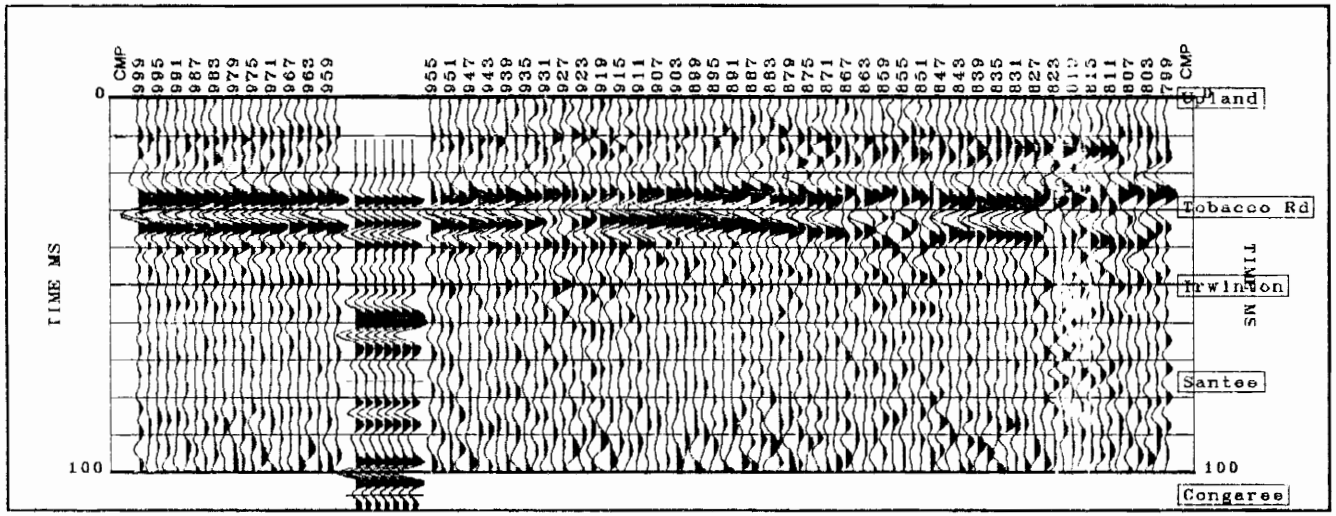

Figure 37. Synthetic seismogram from well PBF-3 correlated with PBF line 12: The correlation with PBF line 12 (stations 200 - 220) is at CMP 957 (station 239). The reference markers are corresponding to Fallow and Price (1992) lithologies. A 105 m datum was used in processing both data sets.

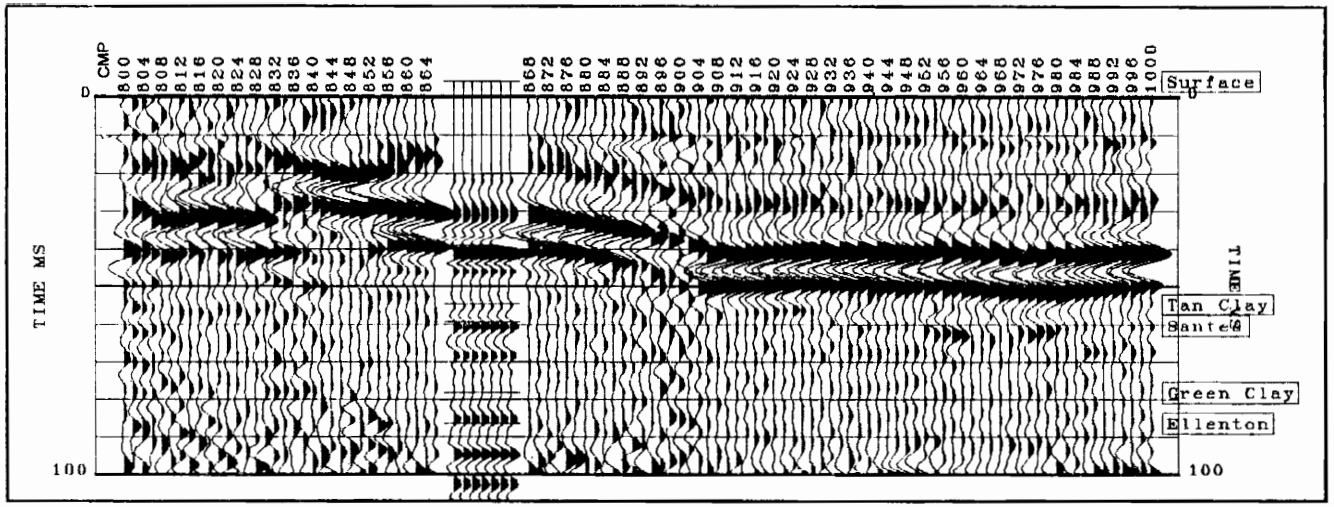

Figure 38. Synthetic seismogram from well PBF-8 correlated with PBF line 11: The correlation with PBF line 11 (stations 200 - 250) is at CMP 866 (station 216.5). The reference markers are corresponding to Berkman (1991) lithologies. A 105 m datum was used in processing both data sets.

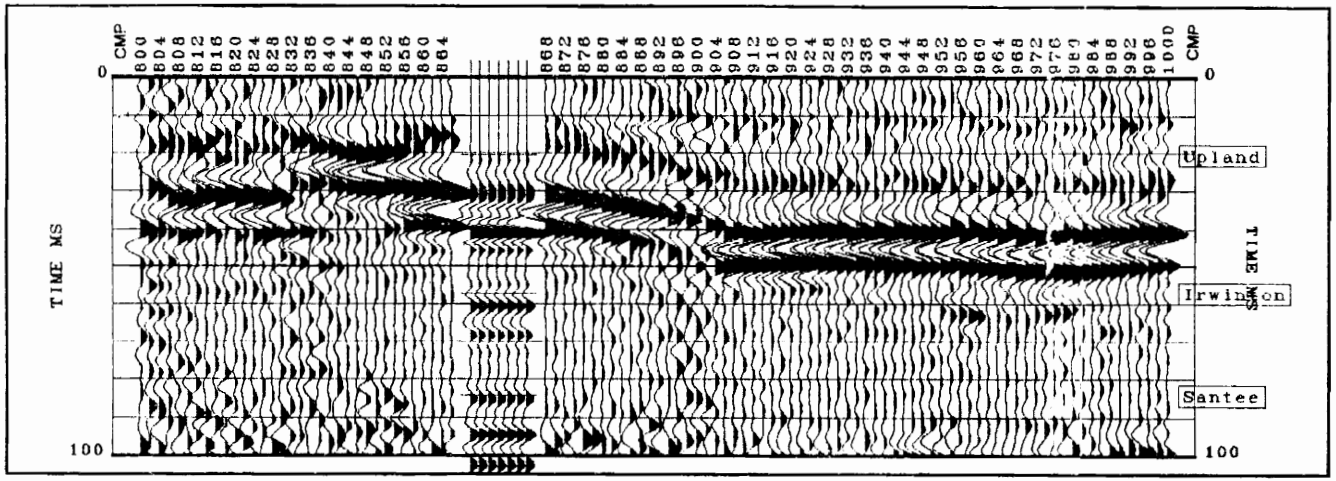

Figure 39. Synthetic seismogram from well PBF-8 correlated with PBF line 11: The correlation with PBF line 11 (stations 200 - 250) is at CMP 866 (station 216.5). The reference markers are corresponding to Fallow and Price (1992) lithologies. A 105 m datum was used in processing both data sets.

Conclusions

The use of refraction stack sections generated from the high resolution reflection seismic data resolves shallower information than what is obtained with the reflection stack sections. Interpretation of the refracted stack sections offers additional constraints about the upward penetration of the Pen Branch Fault. All of the reprocessed lines suggest that the shallowest event recovered in refracted stack sections is affected by faulting and/or deformation. Displacement along the zone is interpreted anywhere from 1 to 5 m. Depths to the shallowest events range from 4 m (PBF lines 6 and 13) to 18 m (PBF line 17).

The faulting shows mainly a reverse sense of motion in the fault zone. On the PBF lines 6, 11 and 13, an offset appears to be on the southern side of a possible stream channel. PBF lines 6 and 13 have the clearest and shallowest offsets. Both exhibit possible reverse offsets for the Pen Branch Fault. The structures on the lines, PBF lines 11, 12, and 17, proved more complex with faulting and deformation and relatively poor resolution. Line PBF 11 has somewhat of a distinct offset showing reverse motion (station 210) but near this location the data is of poor quality. When the location of the Pen Branch Fault from other studies is compared with the results of this study, for the most part, this has helped in narrowing possible offsets that would be associated with the Pen Branch Fault. When projecting the location of the fault in PBF line 12 from other interpreted lines having clear offsets, the fault should pass through the beginning of the line between stations 101 - 170, where there is no strong evidence of an offset in the refraction stack. Some interpretations (Sen, 1991; Çoruh and Costain, 1994) lead to a projection of the Pen Branch Fault to station 210 on PBF line 12, where a slight offset of reverse motion may be evident in the refraction stack. Last, PBF line 17 resulted in an undulating and discontinuous refractor. Using other line interpretation a possible location for the Pen Branch Fault is interpreted at a possible reverse offset at station 215 of PBF line 17. For each line, a

possible offset is interpreted that shows reverse motion and may be associated with the main Pen Branch Fault. The displacements associated with the Pen Branch Fault decrease northeast to southwest from PBF line 6 to PBF line 17 from 5 m to 1 m. This decrease from the northeast to southwest corresponds to the possibility of a reverse of motion between PBF lines 3 and 15 (Çoruh and Costain, 1994), where there may be a zero offset between these two lines. The offsets would be decreasing to a point of zero offset towards PBF line 15. Also, these smaller displacements correspond to the fact that the Pen Branch Fault offsets decrease through the younger sediments.

As to the evidence for a capping layer for the fault thus determining the age of movement, the correlations that were done with log data generally indicated that the refraction events might be associated with the Dry Branch Formation (Tan Clay (Twiggs Clay) and Irwinton Sand), the Tobacco Road Sand (Late Eocene) and possibly the earlier Santee (Middle Eocene). The presence of features that might be caused by stream channeling gives a possible indication of a fluvial environment such as the Upland Unit sediments, which are not widespread in the site. Unconformably overlain by these sediments, the Tobacco Road Sand sediments have thickness variations caused by stream channels. It would be interpreted that displacement in the ACP sediments penetrates at least through the Late Eocene. No flat lying layer or undeformed/unfaulted horizon is imaged to cap the fault in the lines processed and interpreted.

References

Berkman, E., 1991. High resolution seismic survey, Pen Branch fault, Savannah River Site, South Carolina: Emerald Exploration Consultants, Inc., Austin, TX. 89p.

Chapman, W. L. and Di Stefano, M., 1989. Savannah River Plant seismic survey, 1987-88, Conoco, Inc. seismic acquisition, research report 1809-005-006-1-89, 110p.

Colquhoun, D. J. and Muthig, Michael G., 1991. Stratigraphy and structure of the Paleocene and Lower Eocene Black Mingo Group, South Carolina. In T. Wright Horton Jr. and Victor A. Zullo (eds.), The Geology of the Carolinas, Carolina Geological Society 15th anniversary volume, Knoxville: University of Tennessee Press, p. 241-250.

Çoruh, C., Costain, J. K. and Stephenson, D.E., 1993. Composite refraction-reflection stack sections: Tracing faults in the Atlantic Coastal Plain sediments (Abstract): Extended abstracts with bibliographies, Society of Exploration Geophysicists 63rd Annual International Meeting and Exhibition Sept. 26-30, 1993, Washington, DC, p 1157-1160.

Çoruh, C. and Costain, J. K., 1994. Upward penetration of the Pen Branch Fault beneath the Savannah River Site, South Carolina: A search for the shallowest flat lying layer by reprocessing of PBF high resolution seismic reflection data: Department of Geological Sciences, Virginia Polytechnic Institute and State Univ., Blacksburg, report prepared for the Westinghouse Savannah River Company, Aiken, South Carolina, 66p.

Çoruh, C., Domoracki, W. J., Costain, J. K., Selvi, O. and Stephenson, D. E., 1995. Composite refraction-reflection stack sections: imaging shallow subsurface features. Proceedings of the symposium on the application of geophysics to engineering and environmental problems, Orlando, Florida, April 23-26. p. 937-946.

Cumbest, R. J., Price, V. and Anderson, E., 1992. Gravity and magnetic modeling of the Dunbarton Triassic basin, South Carolina: Southeastern Geology, v. 33, n. 1, p. 37-51.

Daniels, D. L., Sites, I. and Popenoe, P., 1983, Distribution of subsurface Lower Mesozoic rocks in the Southeastern United States, as interpreted from regional aeromagnetic and gravity maps; *in* Studies related to the Charleston, South Carolina earthquake of 1886- Tectonics and Seismicity: U.S. Geological Survey Prof. paper 1313-K, p.1-24.

Domoracki, William J., 1995. A geophysical investigation of geologic structure and regional tectonic setting at the Savannah River site, South Carolina. Ph.D. dissertation, Virginia Tech. 236 p.

Fallow, W.C. and Price, Van, 1992. Outline of the stratigraphy at the Savannah River Site. In Wallace Fallow and Van Price (eds.), Geological investigations of the Central Savannah River area, South Carolina and Georgia, Carolina Geological Society field Trip guidebook, Nov. 13-15, 1992, p. B-II-1-33.

Fallow. W.C., Price, Van and Thayer, Paul A., 1992. Stratigraphy of the Savannah River Site, South Carolina. In Victor A. Zullo, W. Burleigh Harris and Van Price (eds.), Savannah River region: transition between the Gulf and Atlantic Coastal Plains, Proceedings of the 2nd Bald Head Island Conference of Coastal Plains Geology, Hilton Head Island, University of North Carolina at Wilmington, Nov. 6-11, 1990, p. 29-36.

Harris, W. Burleigh and Zullo, Victor A., 1992. Sequence stratigraphy of the Paleocene and Eocene deposits in the Savannah River region. In Victor A. Zullo, W. Burleigh Harris and Van Price (eds.), Savannah River region: transition between the Gulf and Atlantic Coastal Plains, Proceedings of the 2nd Bald Head Island Conference of Coastal Plains Geology, Hilton Head Island, University of North Carolina at Wilmington, Nov. 6-11, 1990, p. 134-142.

Nystrom Jr., Paul G., 1992. Middle and Late Wisconsinan radiocarbon dates of peat in the Upper Three Runs and Tinker Creek alluvial sediments: constraints on rates of incision and sedimentation. In Wallace Fallow and Van Price (eds.), Geological investigations of the Central Savannah River area, South Carolina and Georgia, Carolina Geological Society Field Trip Guidebook, Nov. 13-15, 1992, p. B IX 1-4.

Nystrom Jr., Paul G., Willoughby, Ralph H. and Price, Lucille Kate, 1991. Cretaceous and Tertiary stratigraphy of the upper Coastal Plain, South Carolina. In T. Wright Horton Jr. and Victor A. Zullo (eds.,), The Geology of the Carolinas, Carolina Geological Society 15th anniversary volume, Knoxville: University of Tennessee Press, p. 221-240.

Palmer, D., 1980. The generalized reciprocal method of seismic refraction interpretation: ed. Burke, K., Tulsa, Society of Exploration Geophysicists, 205 p.

Palmer, D., 1981. An introduction to the generalized reciprocal method of seismic refraction interpretation: Geophysics, v. 46, n. 11, p. 1508-1518.

Palmer, D., 1986. Refraction seismics the lateral resolution of structure and seismic velocity: eds., Helbig, K. and Treitel, S., London, Geophysical Press, 269 p.

Peterson, T. A., Brown, L. D., Cook, F. A., Kaufman, S. and Oliver, J. E., 1984, Structure of the Riddleville basin from COCORP seismic data and implications for reactivation tectonics: Journal of Geology, v. 92, p. 261-271.

Prowell, D. C. and Obermeier S. F., 1991. Evidence of Cenozoic tectonism. In T. Wright Horton Jr. and Victor A. Zullo (eds.), The Geology of the Carolinas, Carolina Geological Society 15th anniversary volume, Knoxville: University of Tennessee Press, p. 309-318.

Robinson, Edwin S. and Çoruh, Cahit, 1988. Basic Exploration Geophysics, New York, John Wiley and Sons, p. 48, 173.

Sen, Ashok K., 1991. Removing near-surface effects in seismic data: application for determination of faults in coastal plain sediments, MS Thesis, Virginia Tech, 98p.

Siple, G. E., 1967, Geology and ground water of the Savannah River Plant and vicinity, South Carolina: U.S. Geological Survey Water Supply Paper 1841, 113p.

Snipes, D. S., Fallow, Wallace C. and Price, Van Jr.,, 1992. Structural Geology of the Savannah River Site in the Coastal Plain of South Carolina. In Victor A. Zullo, W. Burleigh Harris and Van Price (eds.), Savannah River region: transition between the Gulf and Atlantic Coastal Plains, Proceedings of the 2nd Bald Head Island Conference of Coastal Plains Geology, Hilton Head Island, University of North Carolina at Wilmington, Nov. 6-11, 1990, p. 33-34.

Snipes, D.S., W.C. Fallow, Price, Van Jr. and Cumbest, R. J., 1993. The Pen Branch fault: documentation of Late Cretaceous-Tertiary faulting in the Coastal Plain of South Carolina, Southeastern Geology, v.33, n.4, p.195-218.

Stieve, A. L., Çoruh, C. and Costain, J. K., 1993, Confirmatory drilling project interim report: USDOE Report WSRC-RP-93-0334, Westinghouse Savannah River Company, Savannah River Site, Aiken, South Carolina, 12p.

Stieve, A. L., Çoruh, C. and Costain, J. K., 1994a, Pen Branch Fault; Confirmatory drilling results (Abstract): Abstracts with Programs, Geological Society of America Southeastern section annual meeting, April 7-8, Blacksburg, VA.

Stieve, A. L., Çoruh, C. and Costain, J. K., 1994b, Confirmatory drilling project final report: USDOE Report WSRC-RP-94-0136, Westinghouse Savannah River Co., Savannah River Site, Aiken, South Carolina, 22p.

Yilmaz, O., 1987, Seismic data processing: Investigations in Geophysics Series Volume 2, ed., S. M. Doherty, Tulsa, Society of Exploration Geophysicists, 526p.

Appendix

Preliminary Testing for Datum Statics Corrections

In order to eliminate elevation and near surface velocity variations effecting the refraction stack sections, a study was carried out to determine whether simple elevation statics or weathering layer plus elevation statics were adequate to apply. For the simple elevation statics,

$$\Delta t = \frac{\Delta z}{v_1}, \tag{1}$$

where Δz is the difference between the datum elevation and the surface elevation and v_1 was the velocity of the first layer (Robinson and Çoruh, 1988).

In the case of the weather layer, considering a vertical raypath through a low velocity weathered zone, statics could be defined by

$$\Delta t = \frac{h}{v_0} + \frac{d - s - h}{v_1}$$

or

$$\Delta t = \frac{d - s}{v_1} + h\left[\frac{1}{v_0} - \frac{1}{v_1}\right], \tag{2}$$

where d and s represented datum and surface elevations for source and corresponding receiver, respectively, while v_0 was the velocity of weathered layer with a thickness of h and v_1 was the velocity of the sub-weathered layer. If there was no weathered layer, $h = 0$, then the above equation reduced to simple elevation correction given in equation (1).

These two methods of static corrections were tested using data from PBF line 13. After selecting a datum that approximated the topography at 94 m, the corrections were calculated using equation (2). The velocities v_0 and v_1 were determined from the direct and refracted arrivals from paper shot records (Figure 40). The thickness of the weathered layer was calculated by using the approximate crossing distance, x_c , of the direct and refracted arrivals (Robinson and Çoruh, 1988):

$$h = \frac{x_c}{2}\sqrt{\frac{v_1 - v_0}{v_1 + v_0}}. \qquad (3)$$

The layer thickness, h, was smoothed twice using a 3-point running average. The smoothed thickness and calculated velocities were used to generate static corrections using equation (2). The computed static corrections were also smoothed with a 3-point running average. The velocities were calculated using full offset range and the data with these statics were called pbf13weather1. The velocities were also calculated using selective offsets in which the statics applied data was called pbf13weather2. Similarly, statics also applied using simple elevation corrections from full range of offsets or selective range and the data with these statics results were pbf13elev1 and pbf13elev2, respectively. Another set of simple elevation statics was computed using a constant velocity of 900 m/s that approximated the velocities from the direct arrivals across the line. The data after these statics were called pbf13v900. After the statics, each data set was sorted by common midpoint. Available residual statics from the previous reflection data (Çoruh and Costain, 1994) were applied to improve the signal-to-noise ratio before velocity analysis was carried out in constant velocity panels using RVMO DISCO module. Data from adjacent CMPs were combined before refraction moveout corrections to improve signal to noise ratio in stacking. A preliminary velocity was chosen from the panels.

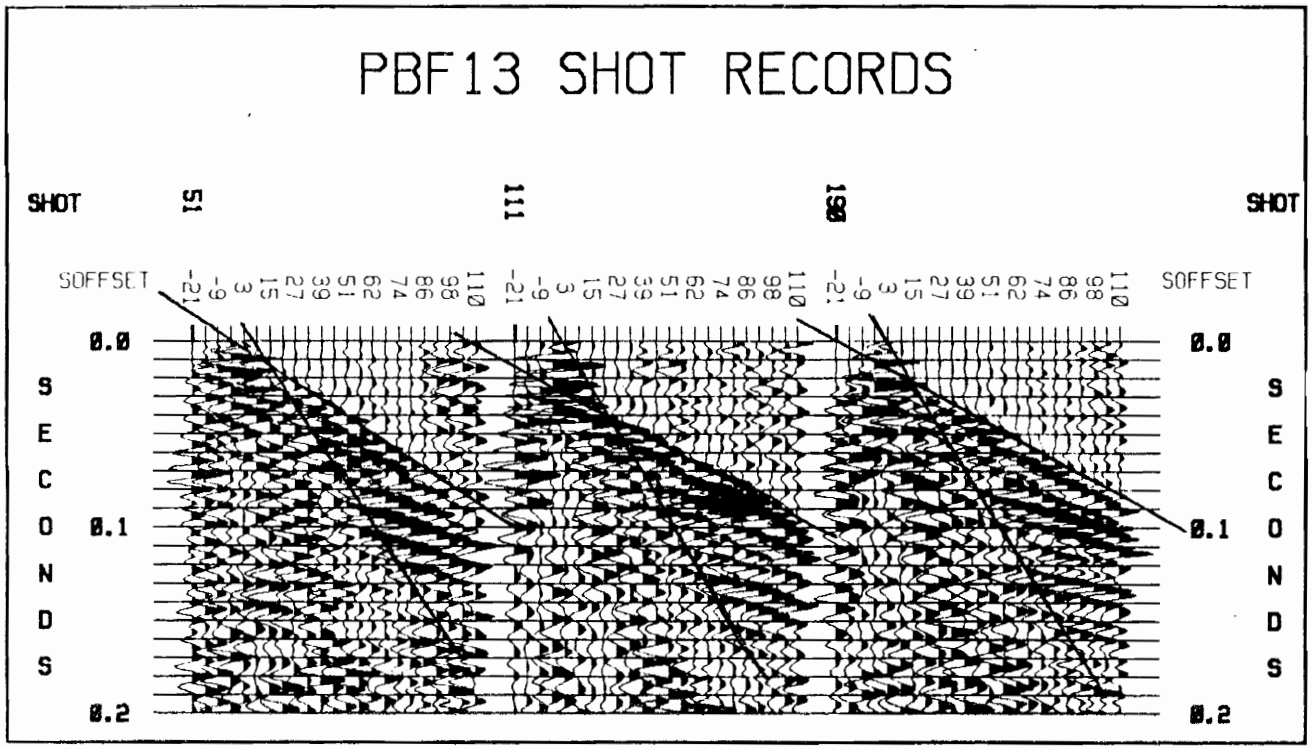

Figure 40. PBF line 13 shot records: Shot records used to determine velocities for datum static correction calculation tests. Lines are drawn to approximate the direct and refracted arrivals.

Preliminary refraction stack sections were created after using RVMO DISCO module with a constant velocity of 1650 m/s obtained from the velocity analysis. These stack sections include predictive deconvolution with a 8 ms gap and 50 ms operator followed by a bandpass filter of 60-70-200-220 Hz (BAND option in the DISCO module FILTER) and AGC balancing with a preliminary window of 200 ms. The tests for selecting these parameters were carried out using interactive FOCUS processing package.

For the preliminary datum correction tests, the use of residual statics increased the resolution of the event recovered in the tests and the deconvolution eliminated the effects of the reverberations. Figures 41 and 42 show after residual statics, deconvolution, filter and AGC for comparison the data sets. After comparing the data sets in Figures 41 and 42, the simple elevation statics corrections were preferred over the statics computed from the weathering layer information.

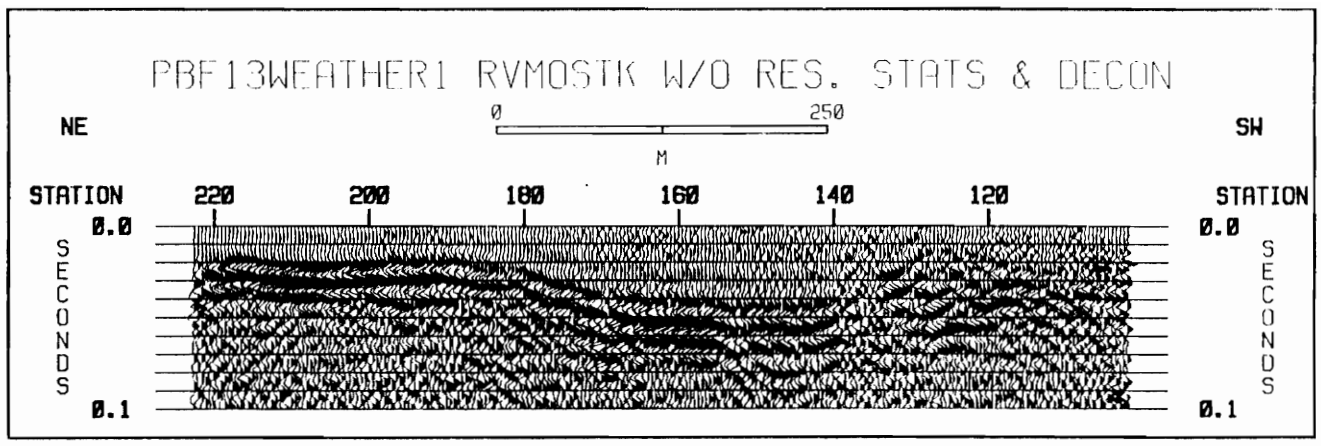

(a)

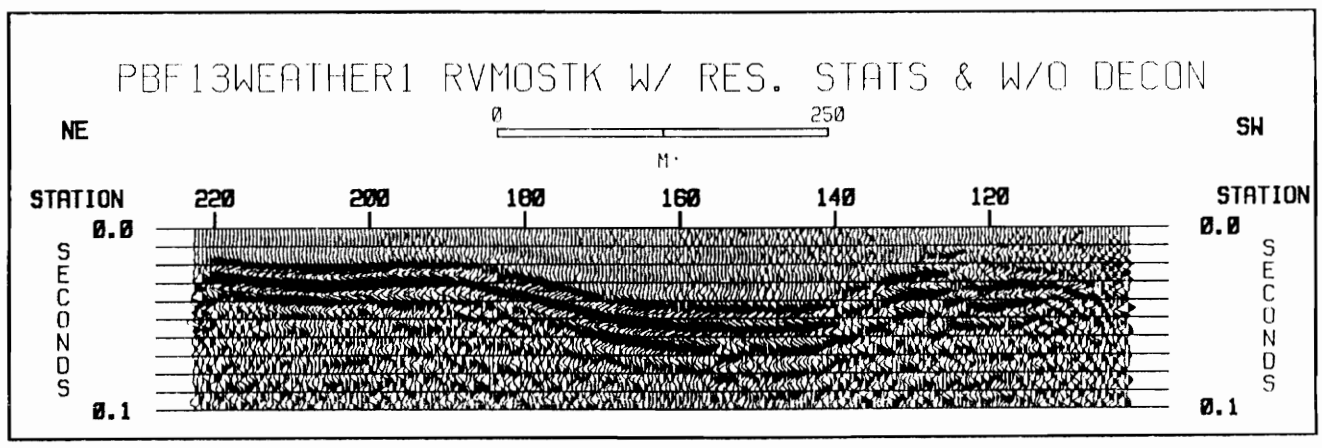

(b)

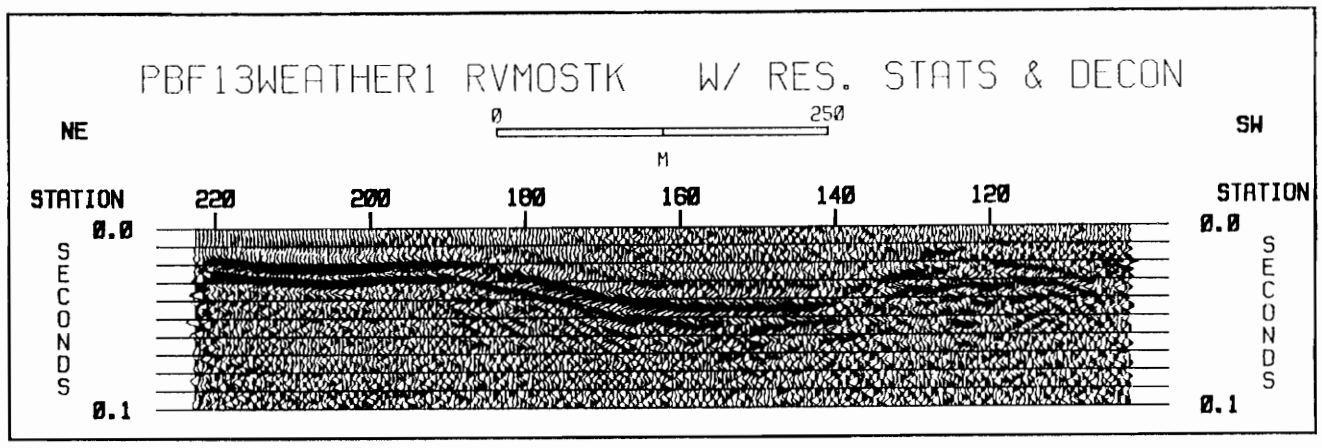

(c)

Figure 41. PBF line 13 stack sections: Datum statics were calculated from a weathered layer model and velocities determined from the full range of offsets. A constant velocity of 1650 m/s was used for the linear refraction moveout correction. The stack sections are shown (a) without residual statics (b) with residual statics and (c) with residual and a predictive deconvolution applied after stack. A filter and amplitude balancing with AGC was applied to each section.

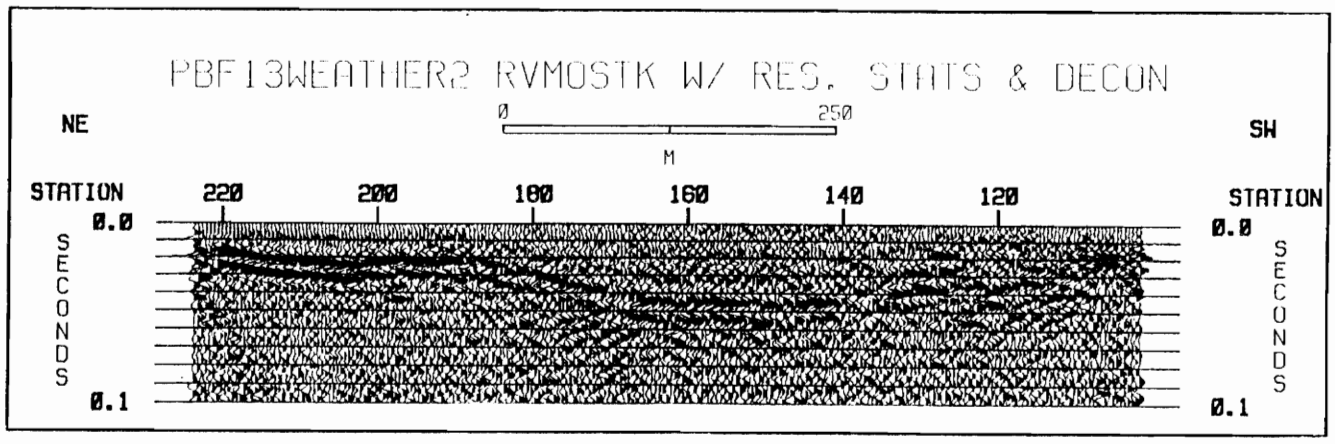

(a)

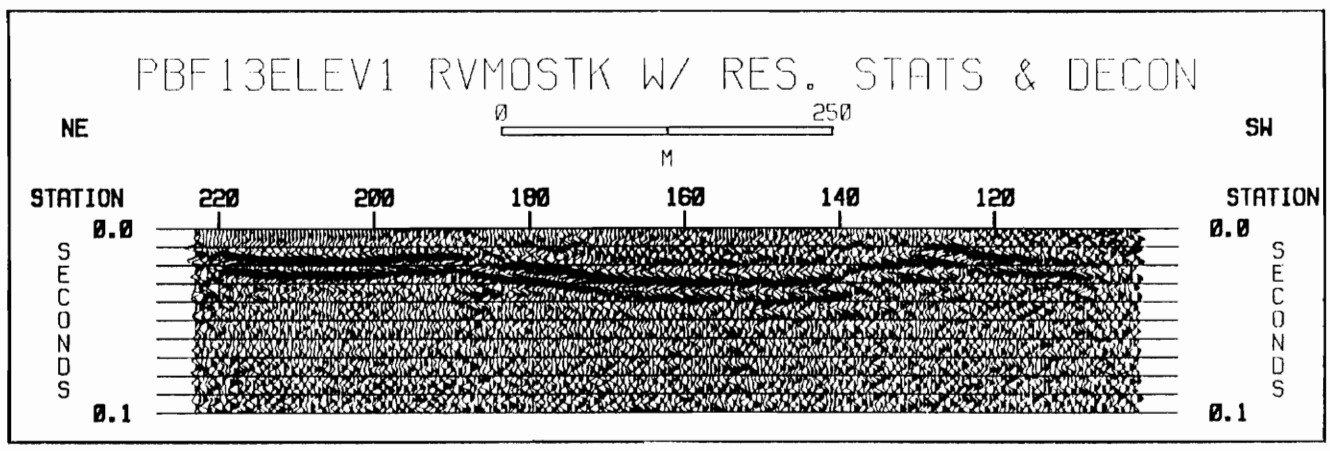

(b)

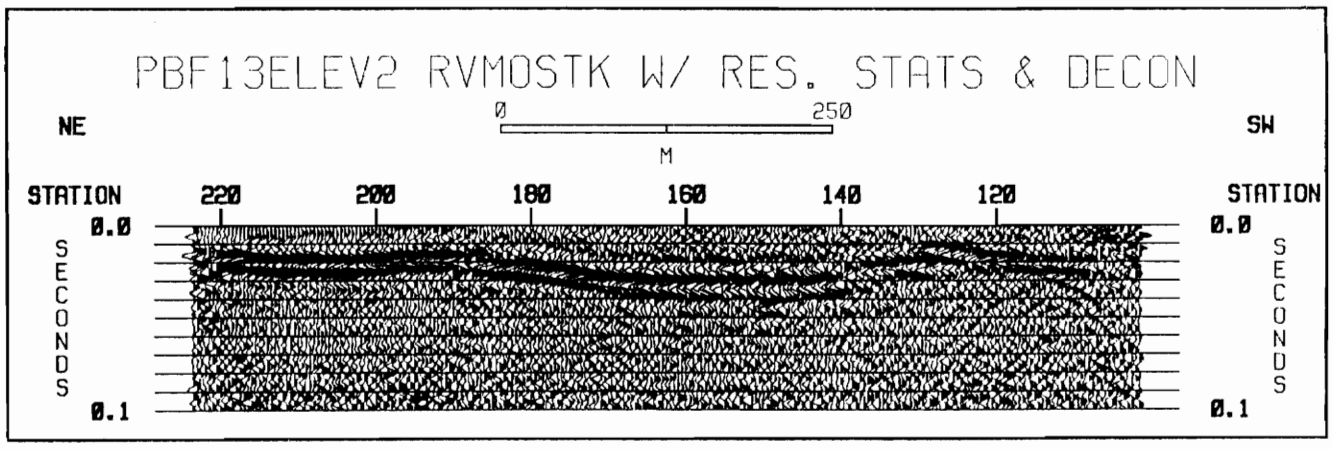

(c)

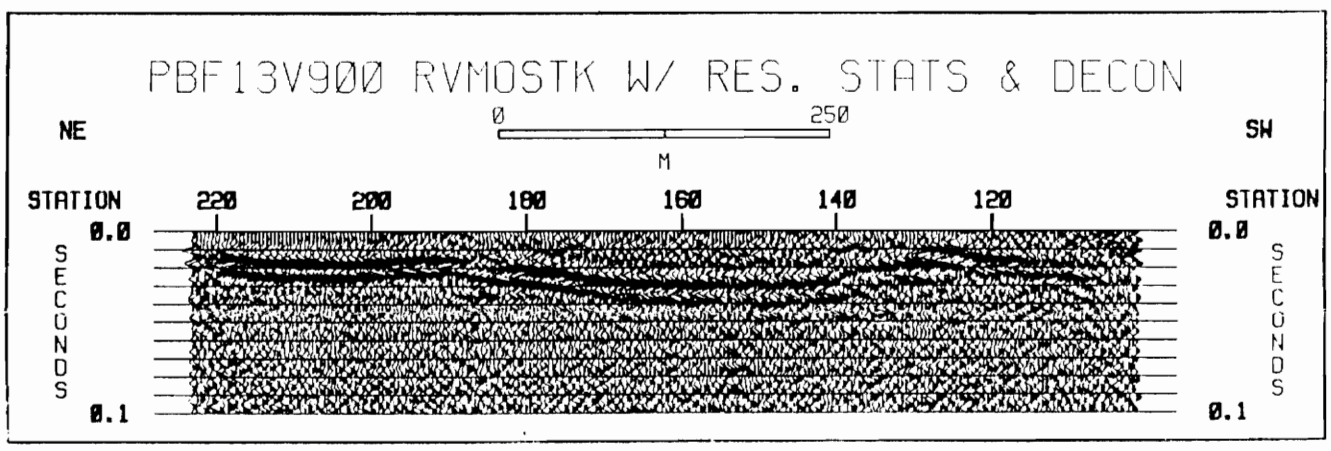

(d)

Figure 42. PBF line 13 stack sections: In (a), datum statics were calculated from a weathered layer model and velocities determined from the selective range of offsets. For (b), (c) and (d), the elevation correction model was used with different velocity determinations. In (b), velocity was determined from the full range of offsets from the direct arrivals, in (c) from the selective range of offsets of the direct arrivals and (d) from an average constant velocity. For all these stacks, residual statics were applied and a constant velocity of 1650 m/s was used for the linear refraction moveout correction before stacking. A predictive deconvolution was also applied after stacking along with a filter and amplitude balancing with AGC.

Vita

Leslie D. Moore was born December 1, 1970 in Lexington Virginia. After graduating high school in 1988 she enrolled in Radford University and received a Bachelor of Science degree in Geology with a specialty in engineering geosciences and a Bachelor of Science degree in Mathematics in May, 1993. In fall of 1993 she enrolled in graduate studies in Geophysics at Virginia Polytechnic Institute and State University. Following completion of her degree she will be employed by Texaco in the offshore division located in New Orleans, Louisiana

Leslie D Moore